International
Progress Report

IPR-07-13

Äspö Hard Rock Laboratory

Äspö Task Force Engineered Barrier System

Modelling of THM-coupled processes for Task 1, Benchmarks 1, using GeoSys/Rock Flow

Thomas Nowak
Federal Institute for Geosciences and Resources
Hannover, Germany

October 2007

Svensk Kärnbränslehantering AB
Swedish Nuclear Fuel
and Waste Management Co
Box 5864
SE-102 40 Stockholm Sweden
Tel 08-459 84 00
+46 8 459 84 00
Fax 08-661 57 19
+46 8 661 57 19

Äspö Hard Rock Laboratory

Report no.
IPR-07-13
No.
F89K
Author
Thomas Nowak
Date
October 2007
Checked by
Jürgen Hesser
Date
2007-10-16
Approved
Anders Sjöland
Date
2007-11-05

Äspö Hard Rock Laboratory

Äspö Task Force Engineered Barrier System

Modelling of THM-coupled processes for Task 1, Benchmarks 1, using GeoSys/Rock Flow

Thomas Nowak
Federal Institute for Geosciences and Resources
Hannover, Germany

October 2007

Keywords: Modelling, Bentonite, Buffer, Thermal, Hydraulic, Mechanical, Unsaturated

Abstract

In 2004 the Swedish Nuclear Fuel and Waste Management Co. (SKB) initiated the project “Task Force on Engineered Barrier Systems”. This project has the objectives to verify the ability to model THM-coupled processes (task 1) and gas migration processes (task 2) in the clay-rich buffer materials. The tasks will be performed on the basis of appropriate benchmarks.

This report describes the modelling of the benchmarks in laboratory scale of task 1 (benchmarks 1) with the code GeoSys/RockFlow. The measured data can be reproduced with the code, in most cases quantitatively, in few cases only qualitatively. Agreement between measured data and calculated data may be enhanced by adjusting parameter values. Thermal, hydraulic, and mechanical processes that are considered to be relevant in these benchmarks are implemented in the code and can be analysed in a coupled way.

Sammanfattning

2004 initierade Svensk Kärnbränslehantering AB, SKB, projektet “Task Force on Engineered Barrier Systems”. Syftet med detta projekt är att verifiera möjligheten att modellera THM-kopplade processer (Task 1) och gasmigrationprocesser (Task 2) i lerbaserade buffertmaterial. Lämpliga laboratorie- och fältförsök ligger till grund för modelleringsuppgifterna.

Denna rapport beskriver modelleringen av benchmarktesterna i laboratorieskala i Task 1 (Benchmark 1) med hjälp av koden GeoSys/RockFlow. Uppmätt data kunde reproduceras med hjälp av koden, i de flesta fallen kvantitativt, i några fall endast kvalitativt. Överensstämmelse mellan uppmätt data och beräknad data kan ökas genom att justera parametervärderna. De termiska, hydrauliska, och mekaniska processer som anses vara relevanta i dessa benchmarktester har implementerats i koden och kan kopplas ihop i analysen.

Contents

1 Introduction

Modelling coupled thermal, hydraulic, mechanical, and chemical processes is of importance for the investigation of different concepts for final repositories. The radioactive waste heats the surrounding system of engineered and geological barriers, and this process shows strong interactions with hydraulic, mechanical, and chemical processes.

In many concepts for final repositories clay-rich materials play an important role as a technical barrier. Due to adsorption of water into the clay mineral lattice these materials are swelling. Changes in water saturation of this technical barrier are caused on the one hand by evaporation of water due to the heat generated by the waste, on the other hand by water from the host rock infiltrating into the technical barrier. The ability to understand and model these reverse processes is of special importance for the performance of a final repository for high active waste.

Several laboratory experiments have been conducted on specimens subjected simultaneously to heating and hydration. The data gained by these experiments (i.e. temperature, relative humidity, total stress) put the numerical tools to the test that are going to be used for the calculation of problems in a larger scale, for example repository-like in situ tests and at last for a repository layout.

This report describes the modelling of some laboratory experiments that have been chosen as benchmarks in the project “Task Force on Engineered Barrier Systems”. For the participation in this project BGR uses the code GeoSys/RockFlow, which is mainly developed in the framework of the DECOVALEX IV project. In chapter 2 the governing equations of the code are presented. Chapter 3, 4, and 5 describe the benchmarks (BM) 1.1.1 to 1.1.3 and how these experiments have been modelled.

2 Code GeoSys/RockFlow

The governing equations, which are essential for the analysis, are detailed hereafter. The description is based on the report for the modelling of Task D in the project DECOVALEX IV (WANG et al. 2005). The description of governing equations is valid for all results documented in this report except for the model of the isothermal test in BM 1.1.2. For modelling this test the two-phase-flow module of RockFlow has been used. A description of this module can be found in THORENZ (2000).

2.1 Non-isothermal flow in porous media

Consider a general case of a flow problem in deformable porous media under the Richard's approximation. With the classical Darcy's law, the large scale water flow $\mathbf{q}_w$ is defined as

$$\mathbf{q}_w = -nS\left(\rho_w \frac{k_{rel}\mathbf{k}}{\mu}\left(\nabla p - \rho\mathbf{g}\right)\right) \tag{1}$$

where S is water saturation, p is the water pressure, ρ is density, n is effective porosity of the media, μ is viscosity, k_{rel} is the relative permeability, g is the gravity force by density and $\mathbf{k}$ denotes permeability tensor. Meanwhile, we consider vapour flow in the filled pores due to molecular diffusion, which is coupled with temperature. Similar to what is defined in (1), the vapour flow is given by

$$\mathbf{q}_v = -D_{pv}\nabla p - f_{Tv}D_{Tv}\nabla T \tag{2}$$

where f_{Tv} is a thermal diffusion enhancement factor taking a value of 1.0 in the present version of the code, D_{pv} and D_{Tv} are diffusion coefficients as

$$D_{pv} = \frac{D_v \rho_v}{\rho_w R T_{abs}}$$
$$D_{Tv} = D_v\left(h\frac{\partial \rho_{vS}}{\partial T} - \frac{\rho_v p}{\rho_w R T_{abs}^2}\right) \tag{3}$$

with h, the relative humidity according to

$$h = e^{p/\rho_w R T_{abs}} \tag{4}$$

R = 461.6 J/kgK, the specific gas constant for water vapour, ρ_{vS}, the saturated vapour density given by

$$\rho_{vS} = 10^{-3} e^{19.891 - 4975/T_{abs}} \tag{5}$$

vapour density $\rho_v = h\rho_{vS}$ and

$$D_V = \tau S_g n 2.16 \times 10^{-5}\left(T_{abs}/273.15\right)^{1.8} \tag{6}$$

τ, the tortuosity, and S_g, the saturation with gas.

The expressions of flow defined in (1) and (2) lead to the governing equation of flow field in the terms of mass balance equation given by

$$n\left[\frac{\rho_w-\rho_v}{\rho_w}\frac{\partial S}{\partial p}+S\beta_p+(1-S)\frac{\rho_v}{\rho_w^2 RT_{abs}}\right]\frac{\partial p}{\partial t}$$

$$+\nabla\cdot(\mathbf{q}_w+\mathbf{q}_v)/\rho_w+S\frac{\partial}{\partial t}(\nabla\cdot\partial\mathbf{u})$$

$$+n\frac{1-S}{\rho_w}\left(h\frac{\partial\rho_{vS}}{\partial T}+\frac{\rho_v p}{RT_{abs}^2}\right)\frac{\partial T}{\partial t}=0 \qquad (7)$$

for any point $x \in \Omega \in \mathrm{R}^n$ with n the dimension of the real space. In eqn. (7), β_p is the storativity. The unknowns of eqn. (7) which have to be solved are saturation of the phase S, fluid pressure p and the coupling term, i.e. temperature and displacement $\mathbf{u}$, deduced by solid deformation. The boundary conditions for this problem can be simplified for this Richard's flow model

$$\mathbf{q}_w\cdot\mathbf{n}=q_\Gamma,\forall x\in\partial\Omega \qquad (8)$$

or Dirchlet type as

$$p=p_\Gamma,S=S_\Gamma,\forall x\in\partial\Omega \qquad (9)$$

This initial-boundary-value-problem can be solved with the corresponding initial condition of unknowns.

2.2 Deformation

Assuming solid grains itself are incompressible, i.e. $\mathrm{d}^s\mathbf{u}/\mathrm{d}^s t = 0$, deformations in porous media can be described by the momentum balance equation in the terms of stress $\boldsymbol{\sigma}$ as

$$\nabla\cdot(\boldsymbol{\sigma}-\chi p\mathbf{I}-\mathbf{p}_{sw}-\alpha\mathbf{D}\Delta T)+\rho\mathbf{g}=0 \qquad (10)$$

χ is Biot's coefficient (equal zero if unsaturated, equal one if saturated), α is the thermal expansion coefficient, $\mathbf{I}$ is the identity, and $\mathbf{D}$ is the elastic material parameter tensor. Density of porous media consists of the portion contributed by liquid and by the portion contributed of solid as $\rho = n\rho^l + (1\text{-}n)\rho^s$. The swelling pressure $\mathbf{p}_{sw}$ in bentonite is calculated by

$$\mathbf{p}_{sw}=S^2 p_{sw}^{\max}\mathbf{I} \qquad (11)$$

2.3 Heat Transport

For the heat transport problem, we consider the convective transport, i.e. the transport of heat by flow. There are two basic kinds of convection recognized such as *forced convection* and *free convection*. In the former, the velocity of convective motion does not have any impact on the temperature of the fluids and the heat energy transport is forced by the flow movement. In the latter, flow velocities are driven solely by buoyancy effects in the fluid, and these are related to temperature change through the

coefficient of thermal expansion. In real ground water systems, there is a mixture of both types of convection. The simple expression of heat flux in forced convection is given by

$$\mathbf{q}_T = -K_e \nabla T + n \sum_{\gamma}^{phase} \left(\rho^{\gamma} C_p^{\gamma} \right) T \mathbf{v} \qquad (12)$$

where K_e is the heat conductivity. The second summand is the flux of heat transported by velocity $\mathbf{v}$ per unit area, and across the entire rock face this flux is reduced by the effective porosity n. With the definition of heat flux (12), the governing equation of the convective heat transport can be derived for any point $x \in \Omega \in \mathrm{R}^n$ as

$$\sum_{\gamma}^{phase} \left(\rho^{\gamma} C_p^{\gamma} \right) \frac{\partial T}{\partial t} - \nabla \mathbf{q}_T + Q_T = 0 \qquad (13)$$

with boundary condition

$$\mathbf{q}_T \cdot \mathbf{n} = q_T \big|_{\Gamma} \text{ , or } T = T_{\Gamma}, \forall x \in \partial\Omega \qquad (14)$$

and initial condition

$$T(x) = T_0(x), \forall x \in \Omega \qquad (15)$$

2.4 Staggered Scheme

The staggered strategy is used for the coupling simulation. The staggered scheme together with the Galerkin finite element approach may damage the mass conservation in the global scale. This is caused by the term in the vapour flux expression (2) concerning the temperature. Applying integration scheme to the flux term of eqn. (7) with a test function v, we have an integration concerning to the second term of (2) as

$$\int_{\Omega} D_{pv} v \nabla (\nabla p) \mathrm{d}\Omega$$

$$\int_{\Omega} D_{Tv} v \nabla (\nabla T) \mathrm{d}\Omega \qquad (16)$$

Integrating eqn (16) part by part leads to

$$\int_{\Gamma} D_{pv} (v \nabla p) \cdot \mathbf{n} \mathrm{d}\Gamma - \int_{\Omega} D_{pv} \nabla v \nabla p \mathrm{d}\Omega \qquad (17)$$

$$\int_{\Gamma} D_{Tv} (v \nabla T) \cdot \mathbf{n} \mathrm{d}\Gamma - \int_{\Omega} D_{Tv} \nabla v \nabla T \mathrm{d}\Omega \qquad (18)$$

Eqn (17) and (18) implies that we have to apply additional Neumann boundary conditions of pressure or temperature to the system equation arising from mass conservation equation (7) to keep mass conservation principle if staggered scheme is applied.

3 Benchmark 1.1.1

Two laboratory experiments have been chosen as BM 1.1.1 for the project Task Force on Engineered Barrier Systems. These experiments have been conducted at the Atomic Energy Company (CEA) in France with the buffer material MX80 (dry density 1.7 g/cm^3) which is considered to be used in the Swedish disposal concept.

3.1 Experiments

In both experiments a specimen (0.203 m in diameter, 0.203 m in height) has been heated from the bottom end stepwise to a temperature of 150 °C while at the top end a temperature of 20.5 °C has been maintained (phase 1). After a steady-state temperature distribution has been reached a water pressure of 1 MPa has been applied at the top end (phase 2), see Figure 3-1. The two specimens (cells) have differed with respect to their initial water content: for cell no. 1 the initial relative humidity has been 60 %, for cell no. 2 it has been 75 %. Temperature, relative humidity, pore pressure, and total pressure have been measured in the specimen. The experiment with cell no. 1 has lasted in total about 365 days and with cell no. 2 in total 290 days. The specimens have been completely constrained by the steel carcase and no additional load has been applied (GATABIN & BILLAUD 2005).

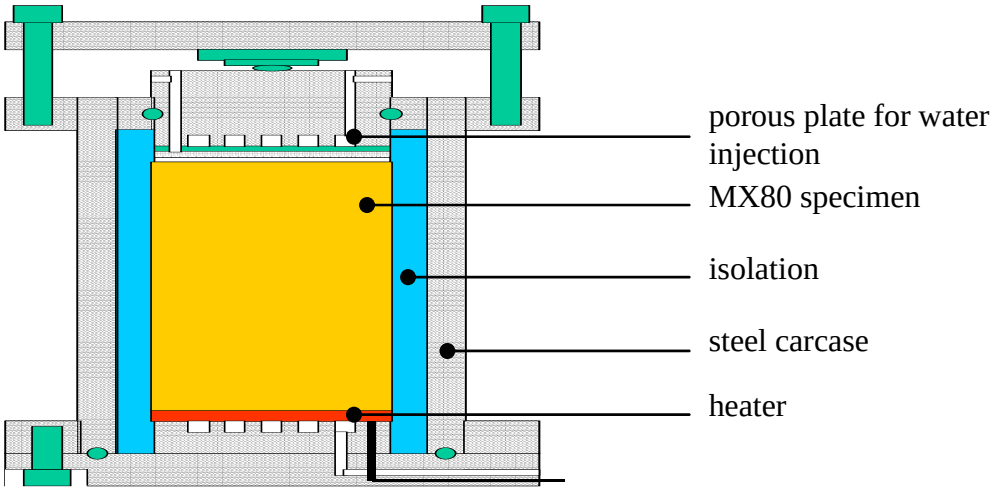

Figure 3-1. *Sketch of the experiments for BM 1.1.1 (modified after GATABIN & BILLAUD 2005).*

The participants of BM 1.1.1 were asked to predict for both specimens the evolution of measured values for a total of 15 temperature sensors, 7 relative humidity sensors, 8 radial pressure sensors, 8 pore pressure sensors, and the total axial pressure. Also the distribution of temperature and relative humidity along the axis of both specimens had to be predicted for six points in time.

3.2 Models

For modelling the BM 1.1.1 one half of the MX80 specimen (axially symmetric problem) has been taken into account. No parts of the test equipment have been included in the model. The specimen has been modelled with 2D elements (plain strain), see Figure 3-2. This simplification leads to deviations with respect to the mechanical response of the specimen to the swelling process, but nevertheless this 2D model can reproduce the effect of swelling qualitatively.

Both cells have been modelled with the same mesh. The models differ with respect to their initial pore water pressure (relative humidity respectively): -69.75 MPa for cell no. 1 and -40 MPa for cell no. 2. Another difference is the course of the time dependent temperature boundary condition along the bottom of the specimen. The onset of hydration (phase 2 of the experiments) has started after about 2710 hours for both cells. Details can be found in GATABIN & BILLAUD (2005).

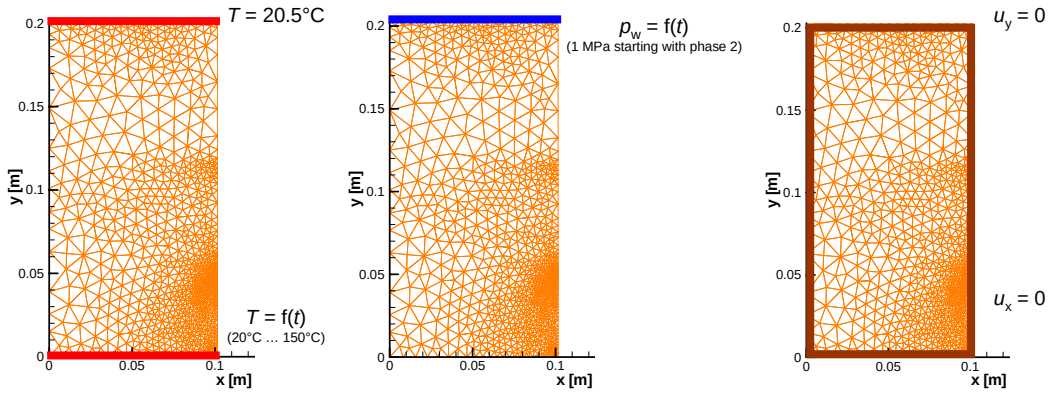

Figure 3-2. *Model for BM 1.1.1: boundary conditions for temperature, water pressure, and displacement.*

The parameter values of the MX80 have been taken as indicated in Table 3-1. With respect to the calculated temperatures the values for heat conductivity and heat capacity are considered to be of minor importance because the temperatures in the small model are governed by the temperature boundary condition. The value for tortuosity has been used as fit parameter to adjust the vapour flow, compare eq. (6).

Table 3-1. Parameter values for MX80 in BM 1.1.1.

parameter	value
permeability [m^2]	6E-21
porosity [-]	0.39
tortuosity [-]	0.4
rel. permeability [-]	$k_{rel} = S_w^3$
capillary pressure [MPa]	$p_c = -248.2*\ln(S_w)$
heat conductivity [W/(m*K)]	0.95
heat capacity [J/(kg*K)]	426
Young's modulus [MPa]	317
Poisson's ratio	0.35
thermal expansion coefficient [K^{-1}]	1.0E-5
max. swelling pressure [MPa]	24.5 (Cell 2: 18.2)

3.3 Results

The results are ordered according to the measured parameter value: first temperature results (for both cells), then relative humidity, total horizontal stress, and total axial stress. Generally, the sensor number correlates with the position in the specimens: the smaller the number, the nearer the sensor is located to the heater. A detailed description can be found in GATABIN & BILLAUD (2005).

3.3.1 Temperature

The measured temperature evolution for all sensors agrees well with the calculated evolution, compare Figure 3-3 for cell no. 1 and Figure 3-4 for cell no. 2. Sensor T0 is located directly at the heater on the bottom. The measured values at this sensor T0 are used as (time dependent) boundary condition for each particular cell (compare Figure 3-2). Sensor T14 is located at the injection end of the specimen where a temperature of about 20.5 °C has been maintained throughout the whole experiment. This value is used as constant boundary condition for both cells. The measured values are shown with bold lines, the calculated values with thin lines. For each sensor measured and calculated values are plotted in the same colour.

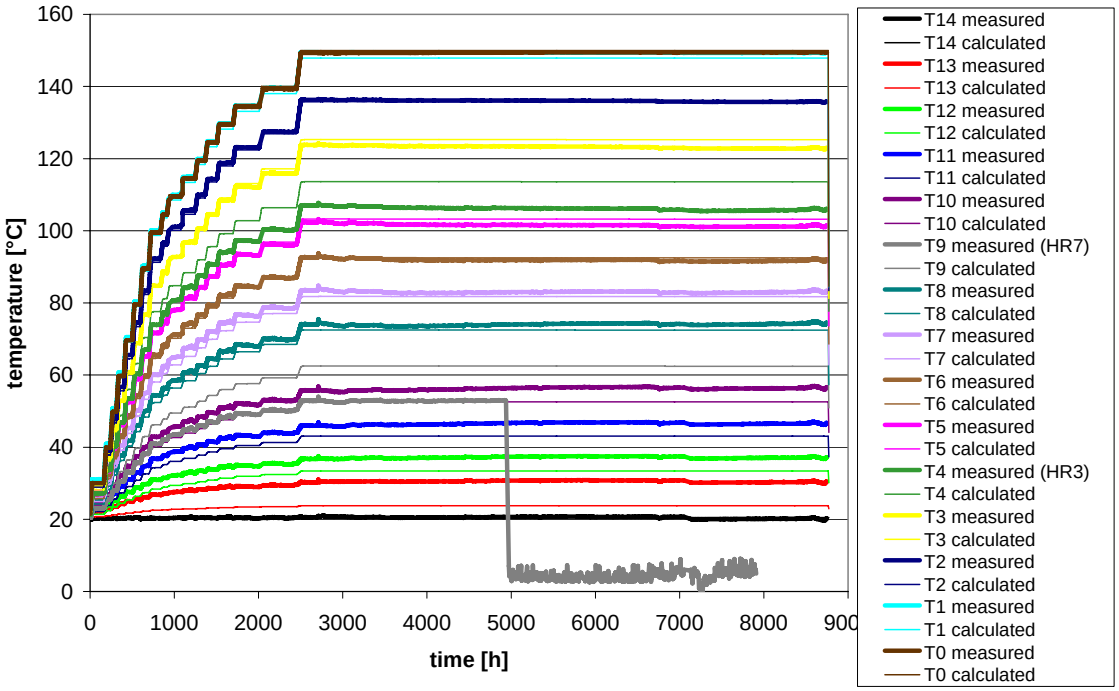

Figure 3-3. *Temperature evolution for cell no. 1.*

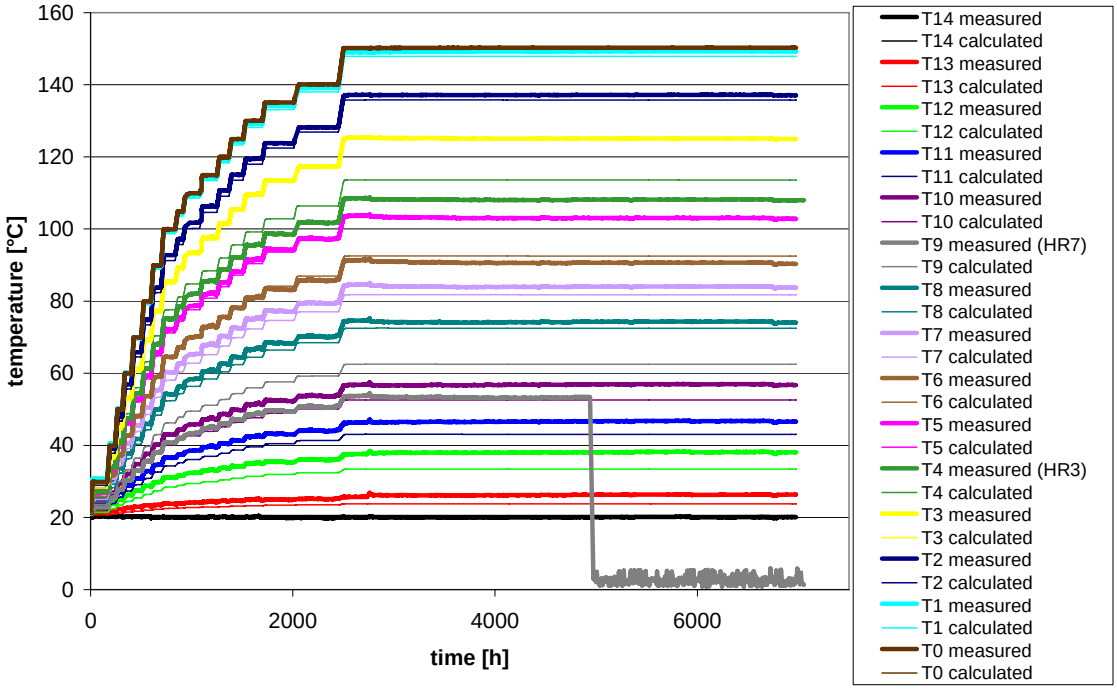

Figure 3-4. *Temperature evolution for cell no. 2.*

In the plot of the temperature distribution it becomes apparent that the calculated values are slightly higher in comparison to the measured values, compare Figure 3-5 for cell no. 1 and Figure 3-6 for cell no. 2. The distribution plots for the 15.09.2003 and later are practically identical and for this reason can hardly be seen.

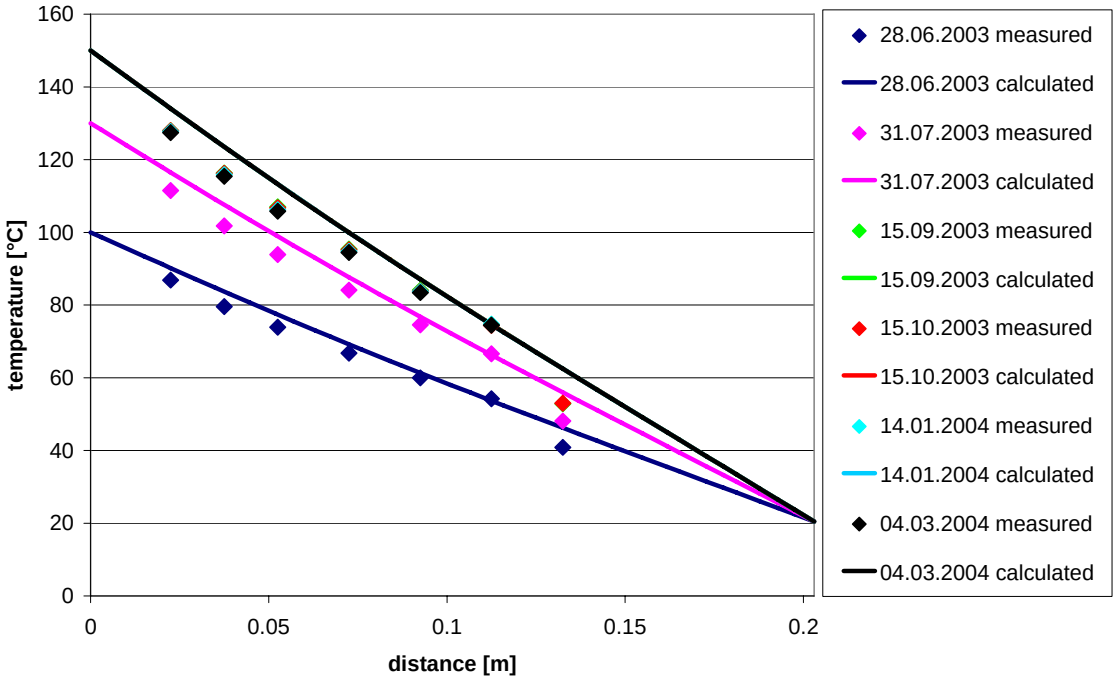

Figure 3-5. *Temperature distribution for cell no. 1.*

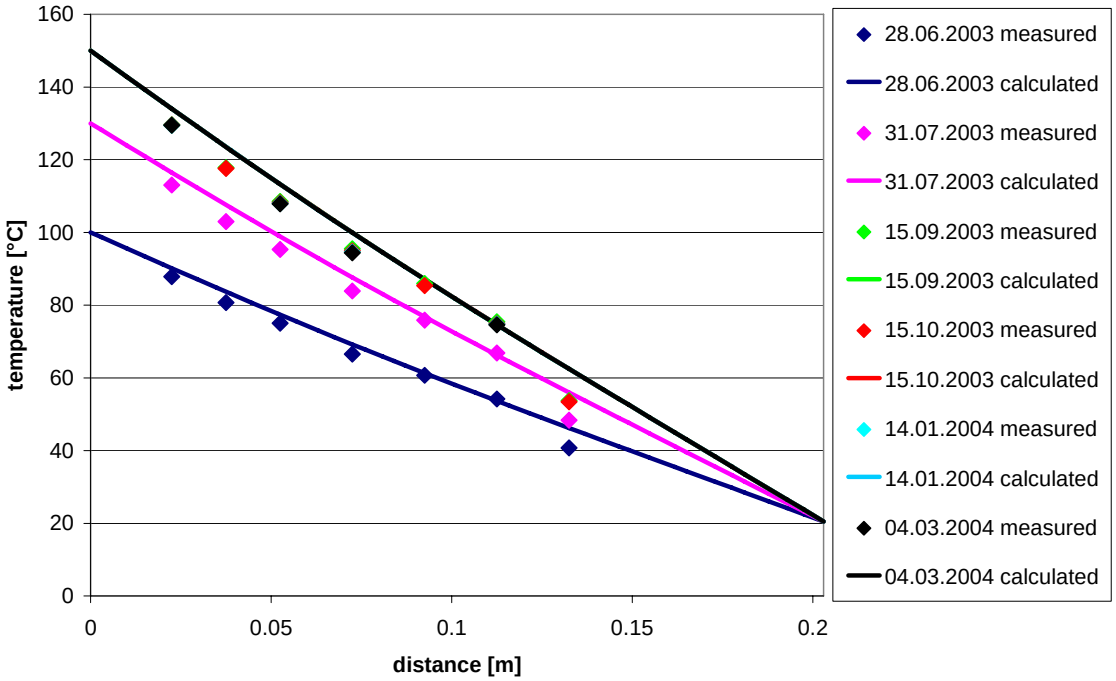

Figure 3-6: *Temperature distribution for cell no. 2*

3.3.2 Relative humidity

The sensors for relative humidity are numbered from HR1 which is located near the (hot) bottom of the specimen to HR7 which is located near the (cold) top of the specimen.

For the cell no. 1 the value of the minimal relative humidity that has occurred for each sensor during the experiment is matched well for the sensors HR1 to HR4 in the warmer areas of the specimen, fairly poor for the sensors HR5 and HR6 in the colder area of the specimen, and fairly good for sensor HR7, compare Figure 3-7.

First the sensors have shown an increase of relative humidity. With increasing temperature (compare Figure3-3) the values for relative humidity have decreased again. In the calculation the minimum relative humidity has occurred much earlier (after roughly 2000 hours) than the point in time that was observed in the experiment (after roughly 3000 hours).

In the calculation all sensors for relative humidity have reacted immediately to the injection of water (in the model the onset of the boundary condition for water pressure respectively) at the beginning of phase 2 of the experiment (compare Figure 3-2). This immediate reaction has also been observed in the experiment by the sensors HR5 to HR7. The sensors HR1 to HR4 have reacted later to this change of the experimental conditions.

Figure 3-8 shows the distribution plot for relative humidity in cell no. 1.

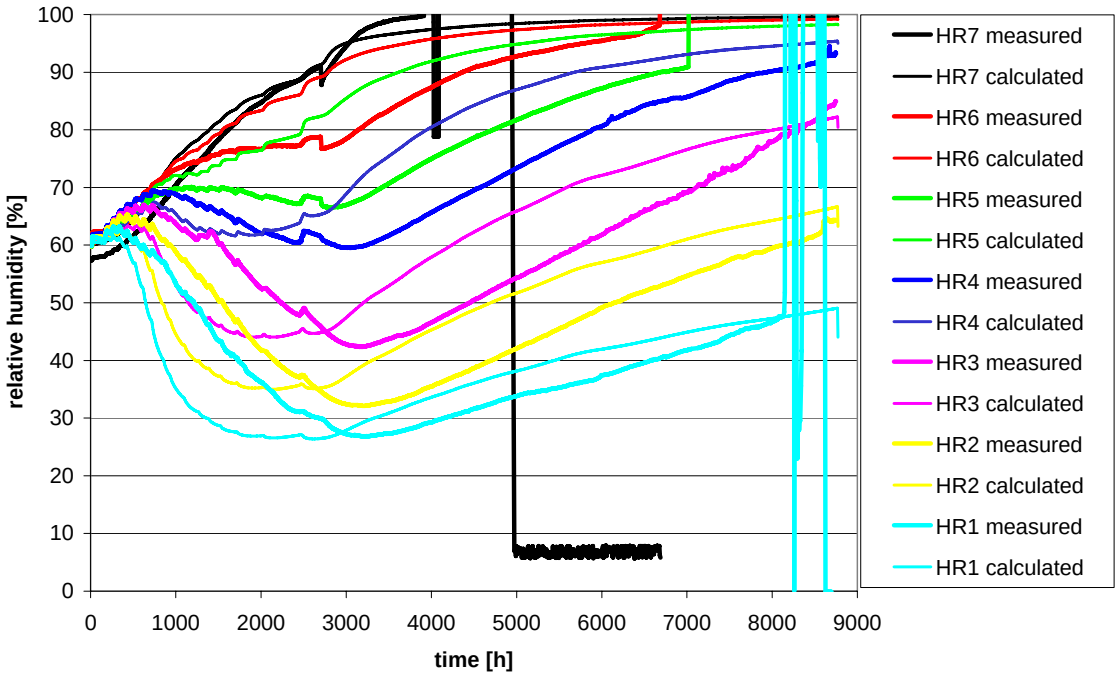

Figure 3-7. *Relative humidity evolution for cell no. 1.*

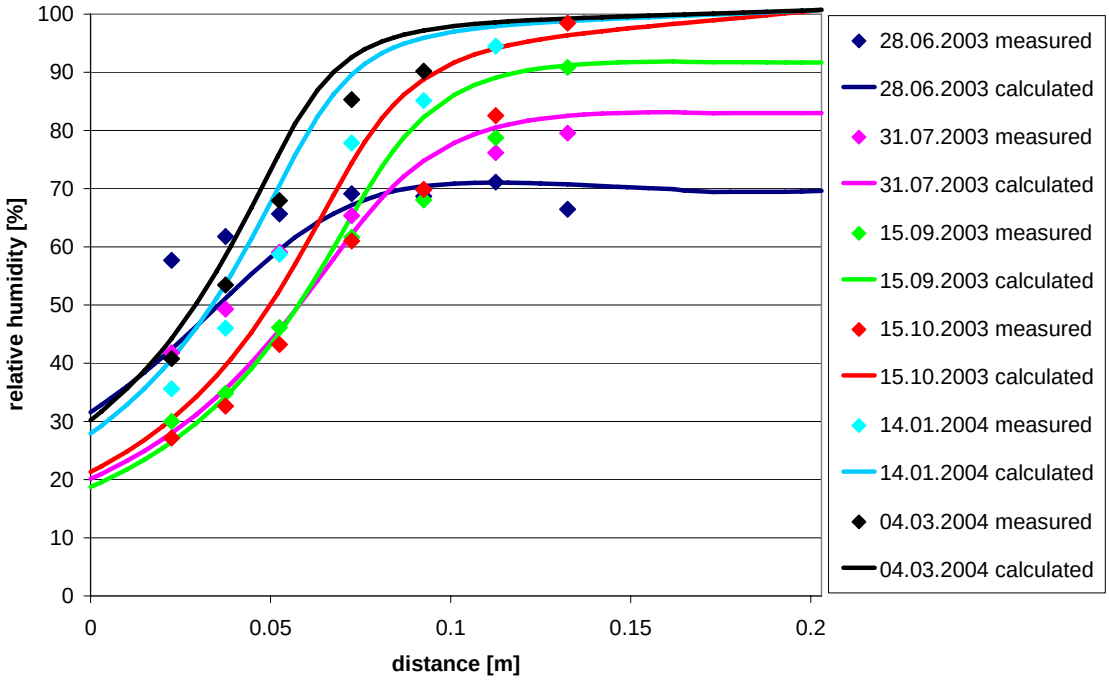

Figure 3-8. *Relative humidity distribution for cell no. 1.*

For cell no. 2 the agreement between measured and calculated data is not as good as for cell no. 1, compare Figure 3-9 and Figure 3-10.

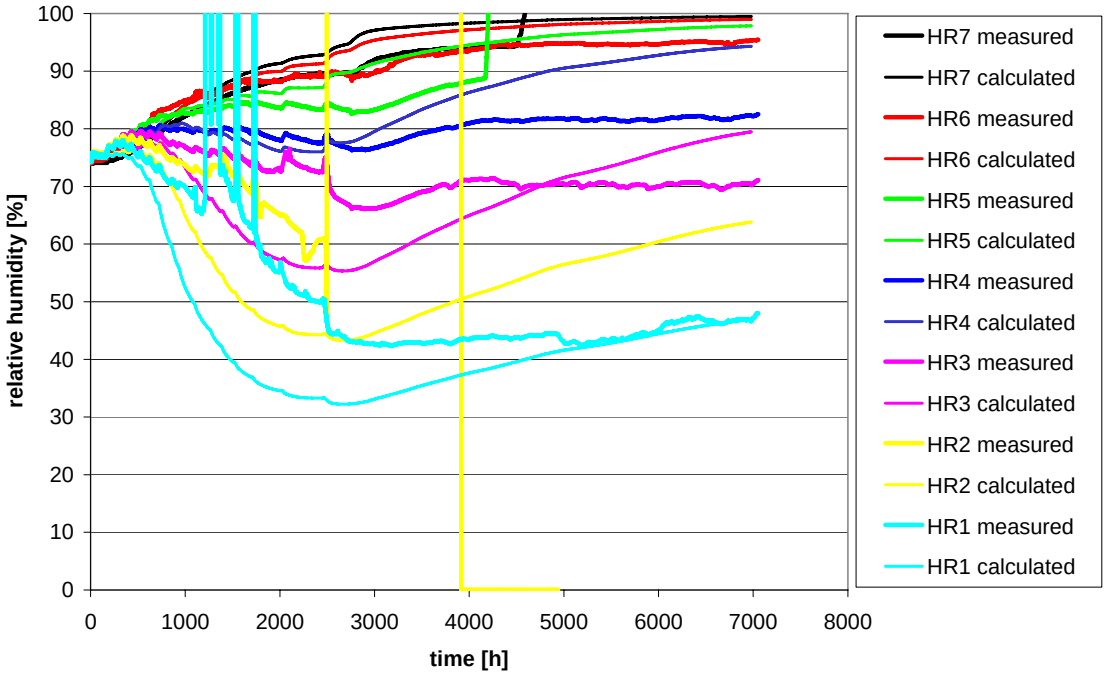

Figure 3-9. *Relative humidity evolution for cell no. 2.*

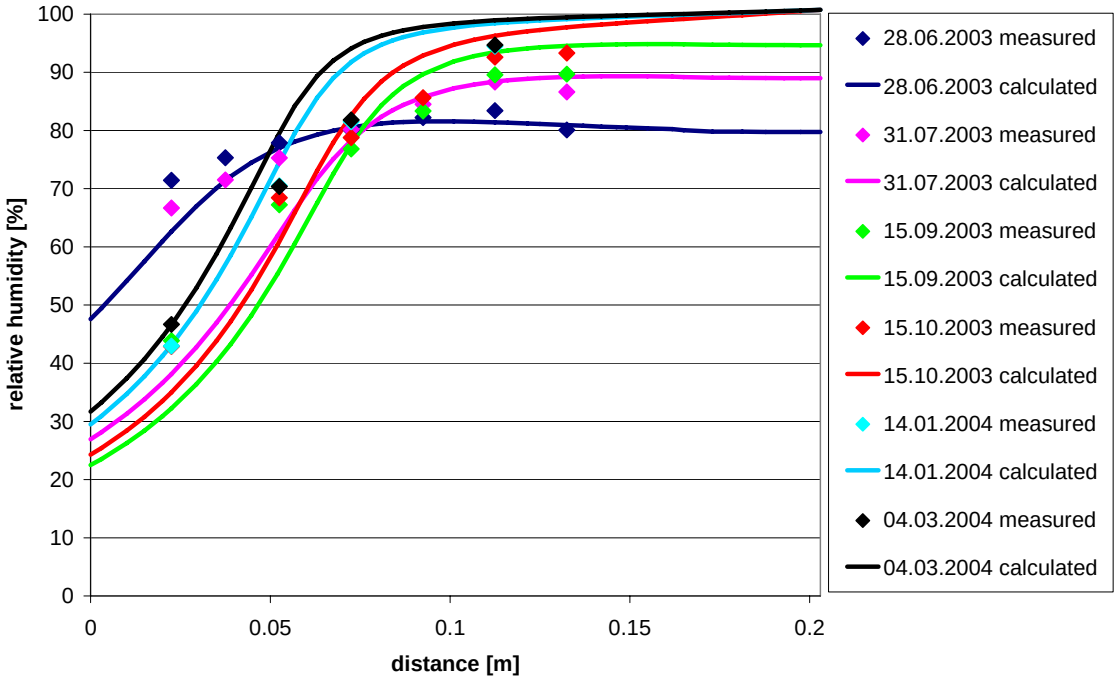

Figure 3-10: *Relative humidity distribution for cell no. 2*

3.3.3 Total radial stress

The sensors for total radial stress are numbered from PT1 which is located near the (hot) bottom of the specimen to PT8 which is located near the (cold) top of the specimen.

For the comparison of measured and calculated data all curves have been shifted to start in the beginning of the experiment at zero: the curves show the changes of the measured and calculated value related to the beginning of the experiment, compare Figure 3-11 for cell no. 1 and Figure 3-12 for cell no. 2.

The curves for the calculation show the change of horizontal effective stresses in the model, the curves for the measurement show the change of radial total stresses. During phase 1 of the experiment the whole model domain has remained unsaturated and Biot's coefficient has been zero in the calculation (compare chapter 2.2). For this reason the measured data of total stress and the calculated data of effective stress are comparable for this phase of the experiment (effective stress equal to total stress as long as Biot's coefficient is zero). In phase 2 water has been injected with 1 MPa from the top and full water saturation has been reached in some parts of the model domain. In this case, Biot's coefficient has been assumed to be equal to one and total stress is then equal to effective stress plus pore water pressure. It is important to notice that the curves for calculated values show effective stresses and the curves for measured values show the total stresses.

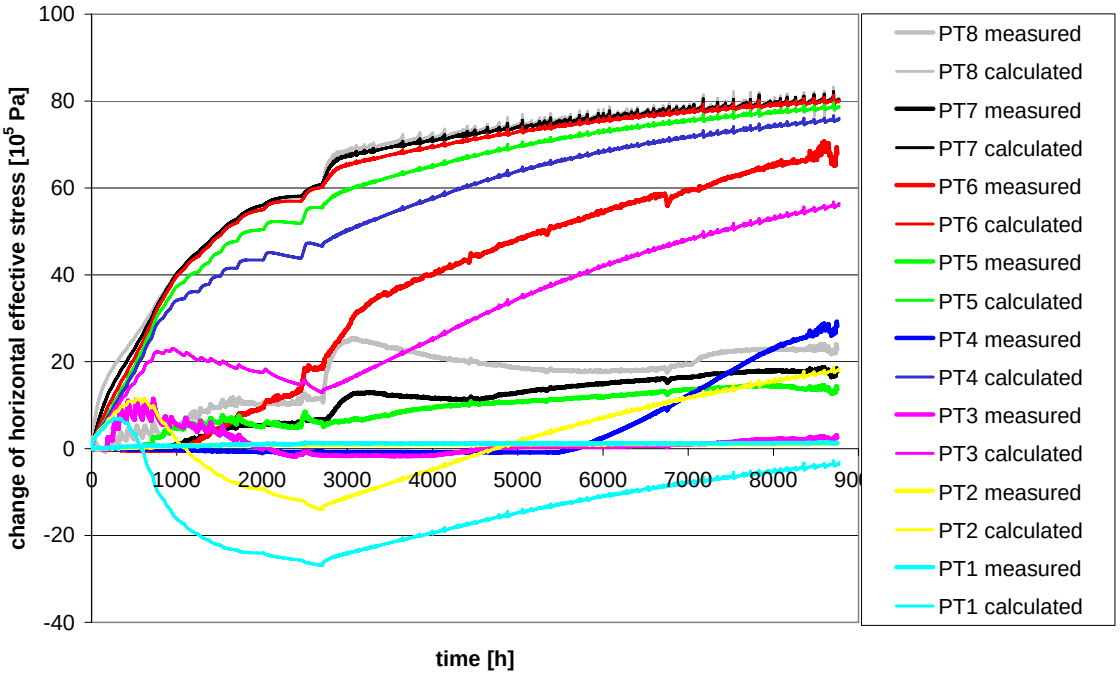

Figure 3-11. *Horizontal effective stress evolution cell no. 1.*

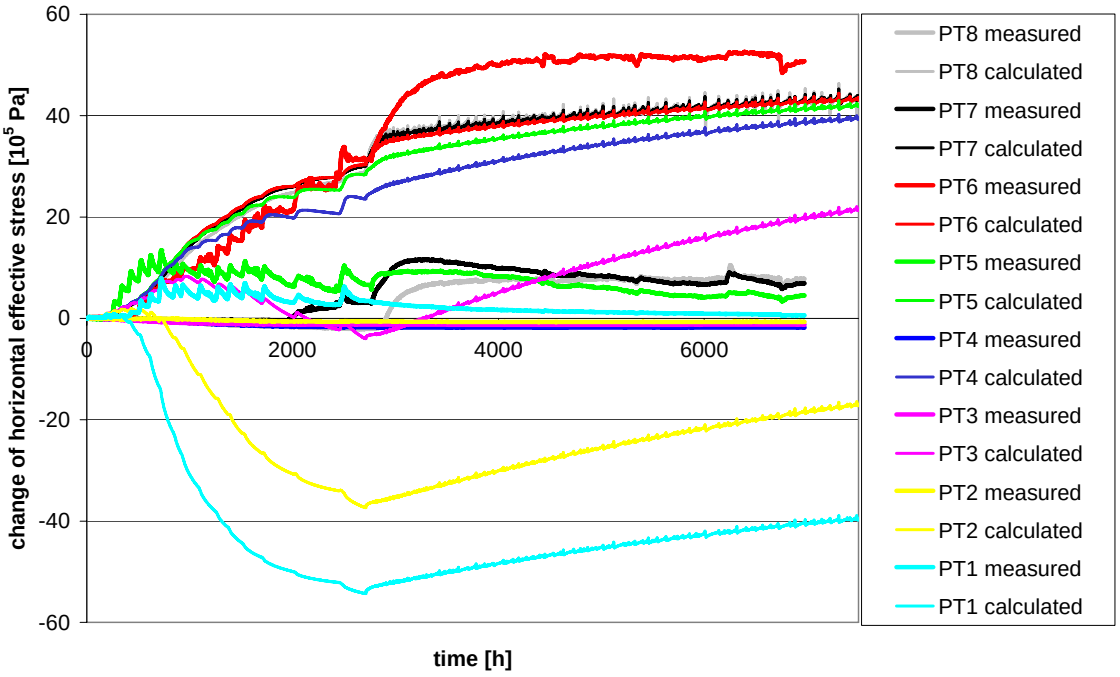

Figure 3-12. *Horizontal effective stress evolution cell no. 2.*

3.3.4 Total axial stress

Beneath the radial stresses the total axial pressure has been measured, compare Figure 3-13 and Figure 3-14. Like in the plots for the radial total stresses it is important to notice that the curves for calculated values show effective stresses and the curves for measured values show the total stresses. Total stress is effective stress plus pore pressure.

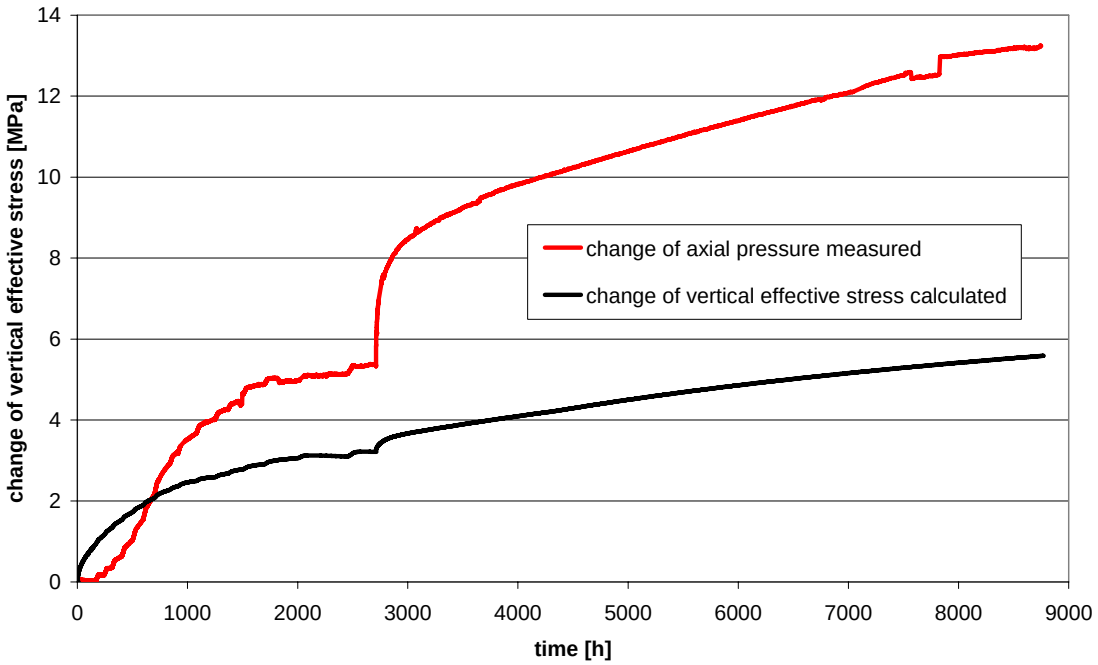

Figure 3-13. *Vertical effective stress evolution cell no. 1.*

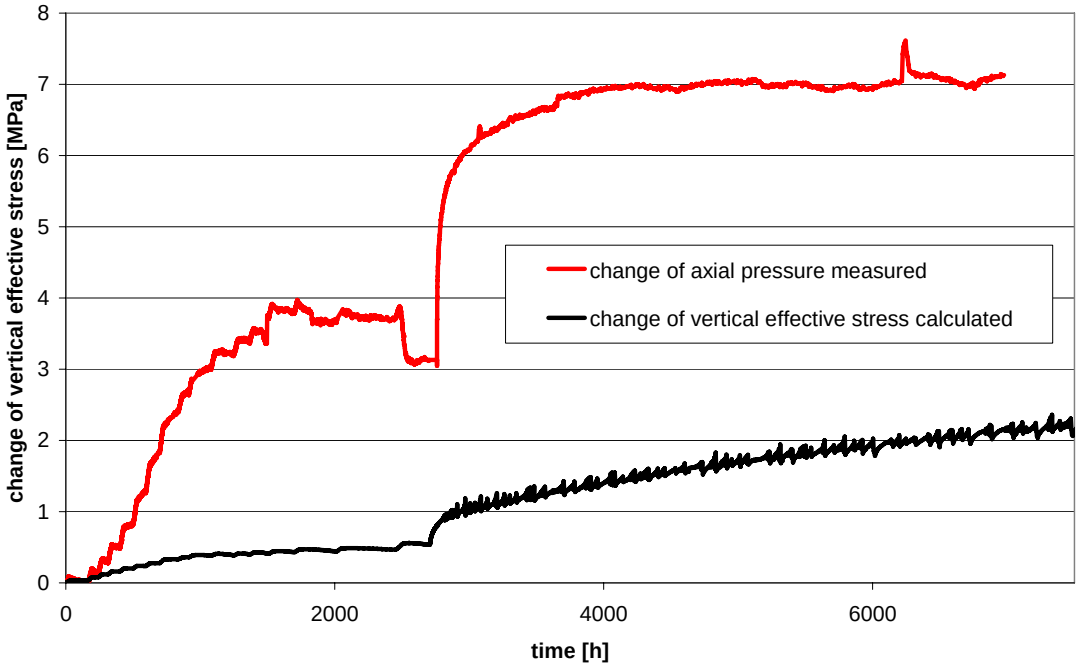

Figure 3-14. *Vertical effective stress evolution cell no. 2.*

3.4 Discussion

With respect to the calculated temperatures the agreement between calculated and measured data is good. In the centre of the specimen predicted temperatures are slightly below the measured values which may be explained by some minor heat loss in the experiment through the isolation and steel carcase.

The sensors for relative humidity first have shown an increase of relative humidity due to the water that has been redistributed by the vapour diffusion from the (hot) bottom (below sensor HR1) to the (cold) top. With increasing temperature the sensors have shown a decrease of relative humidity indicating the further redistribution of water to the top of the specimen. The results for both cells indicate that the water is more mobile in the model than it has been found to be in the experiments. This discrepancy may be solved by adjusting the parameter values controlling either the vapour and/or the water flow. Qualitatively the redistribution of water can be described quite well with the model.

For several reasons, an interpretation of calculated and measured stresses is difficult. One reason is the underlying technique of measurement, which cannot detect tensile stresses in the specimen (shrinkage of the specimen, respectively). In the calculation the water content has decreased in the lower (hot) part of the specimen, and also in the experiment a decrease of relative humidity has been measured. For this reason one can assume that shrinkage of the specimen has occurred in the experiment.

In the experiment a higher total axial pressure has been found in cell no. 1 compared to cell no. 2. Cell no. 1 had a lower initial water content, for this reason it could take up more water until saturation and accordingly swelling pressure has been higher either in the experiment and in the model.

The plane strain assumption of the model is not appropriate for the experiment. With the current version of the code this problem could have been solved by modelling the experiment in 3D (which is available in GeoSys/RockFlow); axially symmetric elements are not available. Nevertheless, the 2D model shows qualitatively the swelling effect.

A further reason causing problems for the interpretation of measured and calculated data is Biot's coefficient: in the calculation it has been assumed to be zero as long as water saturation is below 1, and it has been assumed to be 1 at full water saturation. There are other assumptions for the course of Biot's coefficient depending on water saturation, but it is difficult (if not impossible) to determine it experimentally. The jump from zero to 1 causes numerical problems (oscillating curves for phase 2, compare Figure 3-11 to Figure 3-14).

4 Benchmark 1.1.2

Two laboratory experiments have been chosen as BM 1.1.2. These experiments have been conducted at the Research Centre for Energy, Environment and Technology (CIEMAT) in Spain with the buffer material FEBEX bentonite (dry density 1.65 g/cm^3).

4.1 Experiments

In both experiments a specimen of 0.07 m in diameter and 0.4 m in height has been used. In one experiment (isothermal test) a water pressure of 1.2 MPa has been applied at the top end of the specimen, in the other experiment additionally the bottom end has been heated to a temperature of 100 °C (thermal gradient test), see Figure 4-1. The specimens have been completely constrained by the steel carcase and no additional load has been applied (VILLAR et al. 2005).

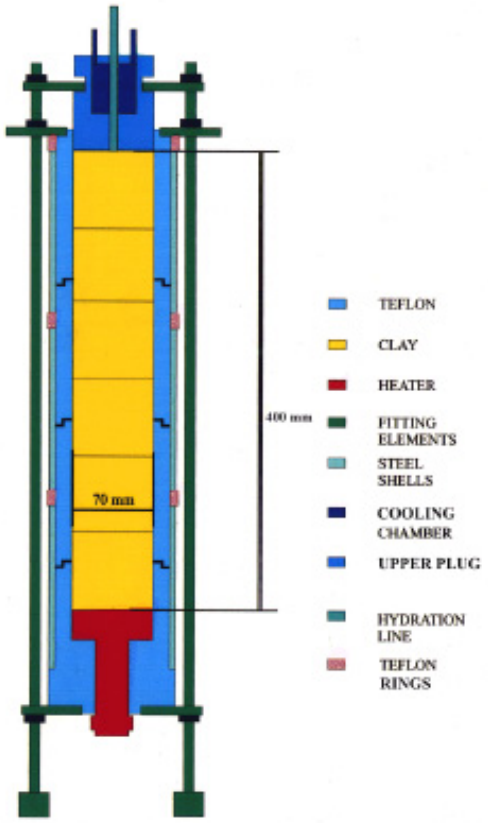

Figure 4-1. *Sketch of the experiments for BM 1.1.2 (VILLAR et al. 2005).*

The participants of BM 1.1.2 were asked to predict for both specimens the evolution of measured values for three temperature sensors and three relative humidity sensors. Also the intake of water for both specimens had to be predicted.

4.2 Models

For modelling BM 1.1.2 two different models have been used.

The isothermal test has been modelled with the two-phase-flow module of RockFlow (THORENZ 2000). The bentonite specimen in the isothermal test has been modelled with 40 1D elements. Boundary conditions in this model are a water pressure of 1.2 MPa on the upper end of the model and an air pressure of 0.1 MPa on the lower end. The hydraulic properties have been the same as in the model for the thermal gradient test (see Table 4-1) except the permeability which has been taken as $2 \cdot 10^{-21}$ m^2 (instead of $1 \cdot 10^{-21}$ m^2 in the thermal gradient test).

For modelling the thermal gradient test of BM 1.1.2 one half of the FEBEX bentonite specimen (axially symmetric problem) has been taken into account. Also the isolation of the test equipment has been included in the model: from the measured temperature values (compare chapter 4.3.1) it was clear from the beginning that considerable heat loss has occurred in the thermal gradient test and that the temperatures in this test have been influenced by seasonal changes of the laboratory temperature. For this reason the Teflon isolation (heat conductivity 0.25 $Wm^{-1}K^{-1}$) and a layer of an artificial material with a heat conductivity like air (0.026 $Wm^{-1}K^{-1}$) has been used in the model together with an adopted time dependent temperature boundary condition, see Figure 4-2. This effort has been made because the reproduction of the measured temperatures in the specimen is a prerequisite for the prediction of vapour flow.

The same hydraulic properties as for the specimen have been assigned to the two isolation materials. This approach has increased the agreement between measured and calculated data and can be justified by the possibility of leakage in the test equipment: the volume of water apparently taken up would result in a degree of water saturation of more than 1 (VILLAR et al. 2005).

The thermal gradient test has been modelled with a mesh of 2D elements. The initial relative humidity is 41.6 % and the initial temperature 23 °C. Details can be found in VILLAR et al. (2005).

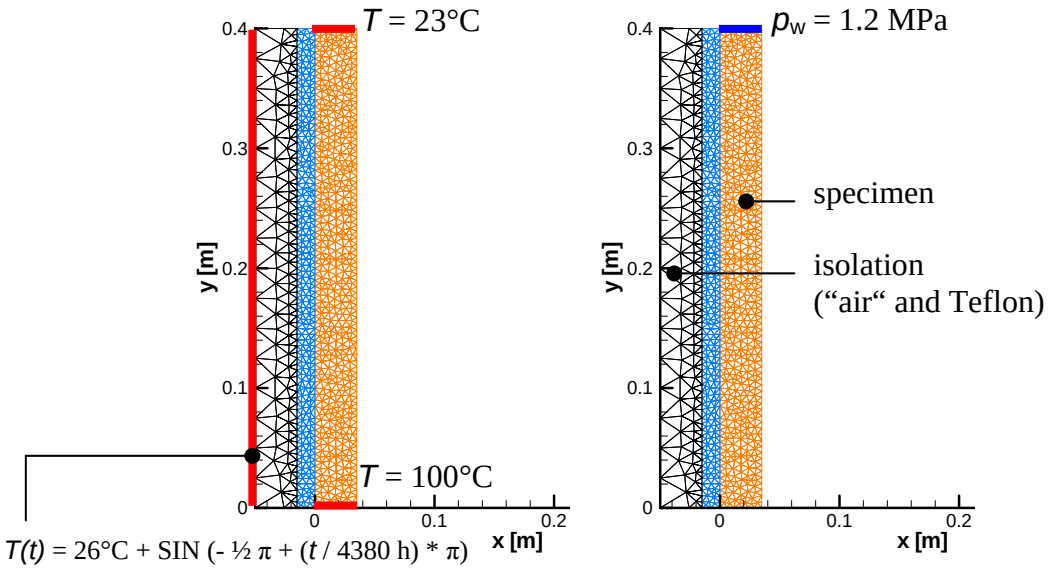

Figure 4-2. *Model for the thermal gradient test of BM1.1.2: boundary conditions for temperature and water pressure.*

The parameter values of the FEBEX bentonite have been taken as indicated in Table 4-1. With respect to the calculated temperatures the values for heat conductivity and heat capacity are considered to be of minor importance because the temperatures in the small model are governed by the temperature boundary condition. The value for tortuosity has been used as fit parameter to adjust the vapour flow, compare eq. (6). The capillary pressure curve has been chosen to fit the empirical relation of water content and suction in the task description (equation 4 in VILLAR et al. 2005)

Table 4-1. Parameter values for FEBEX bentonite in BM 1.1.2.

parameter	**value**
permeability [m^2]	1E-21
porosity [-]	0.39
tortuosity [-]	1
rel. permeability [-]	$k_{rel} = S_w^3$
heat conductivity [W/(m*K)]	0.95
heat capacity [J/(kg*K)]	426
Young's modulus [MPa]	317
Poisson's ratio	0.35
thermal expansion coefficient [K^{-1}]	1.0E-5

4.3 Results

The results are ordered according to the measured parameter value: first temperature results (for the thermal gradient test), then relative humidity, and water intake.

The sensors are located at 10 (sensor no. 3), 20 (sensor no. 2), and 30 cm (sensor no. 1) from the (heated) bottom.

4.3.1 Temperature

The measured temperature evolution for all sensors agrees well with the calculated evolution for the thermal gradient test, compare Figure 4-3.

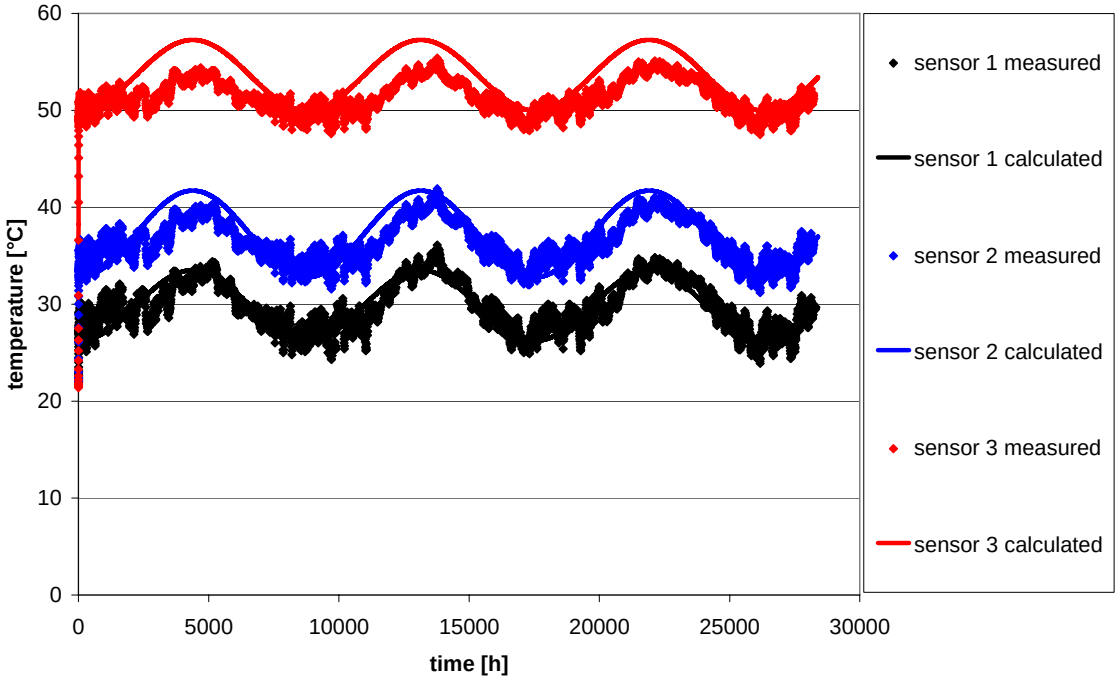

Figure 4-3. *Temperature evolution for the thermal gradient test.*

4.3.2 Relative humidity

For the isothermal test the evolution of measured relative humidity is matched well with the calculation for all sensors, compare Figure 4-4.

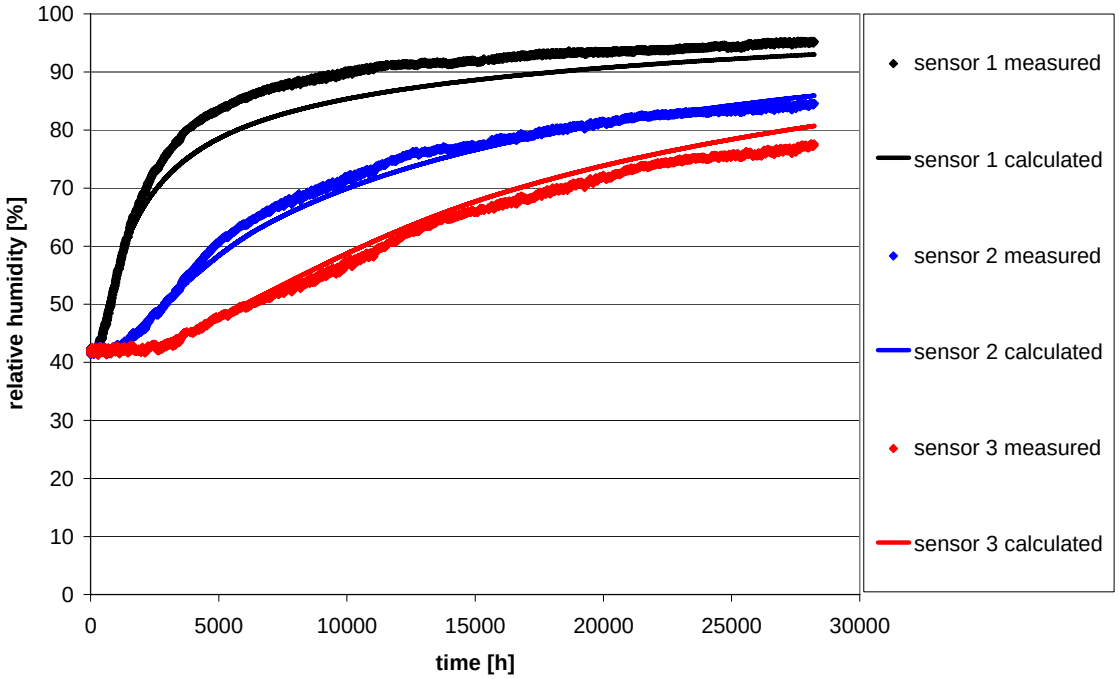

Figure 4-4. *Relative humidity evolution for the isothermal test.*

For the thermal gradient test the agreement between measured and calculated data is good for the sensor no. 1 (10 cm from the top of the specimen where the water is injected). The agreement is fairly poor for the sensors no. 2 and 3. The unsteady temperatures affect the calculated relative humidity much more than it was found in the experiment.

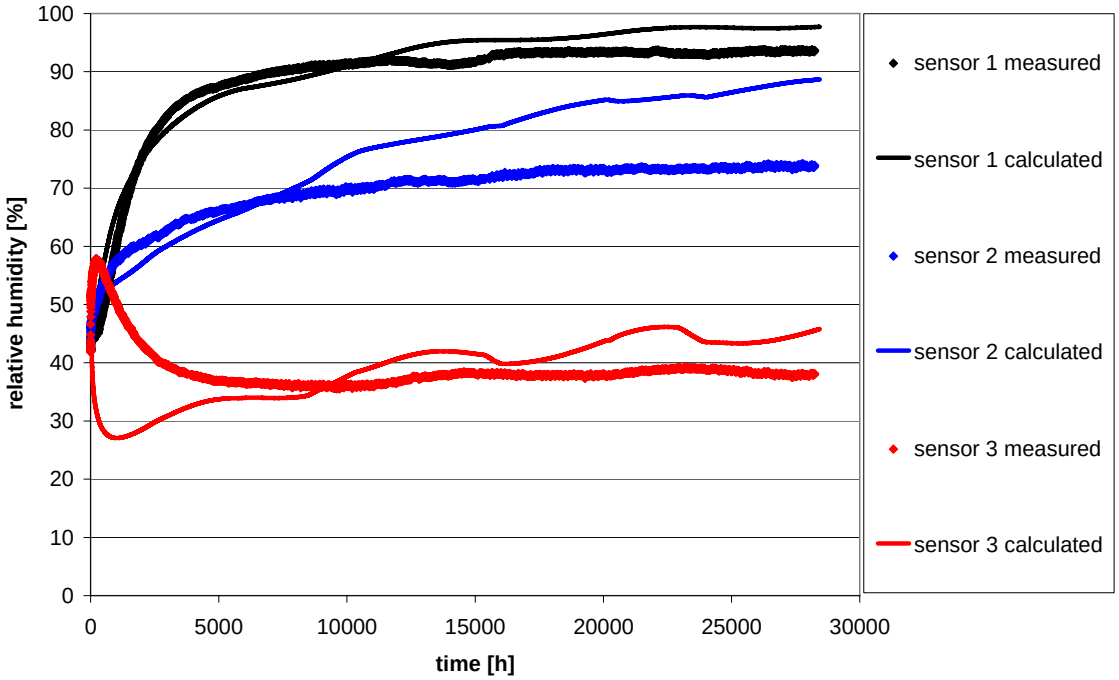

Figure 4-5. *Relative humidity evolution for the thermal gradient test.*

4.3.3 Water intake

The calculated evolution of water intake in the isothermal test (1D two-phase-flow) is clearly below the measured evolution of water intake, compare Figure 4-6.

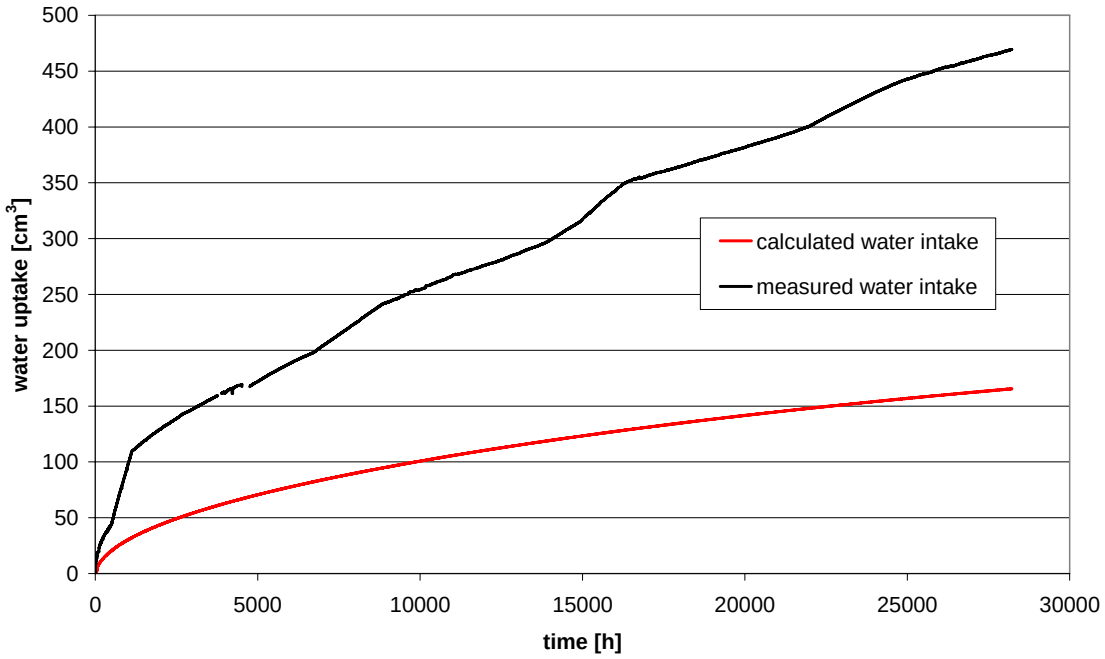

Figure 4-6. *Water intake evolution for the isothermal test.*

For the rating of the measured data it is worthwhile to estimate roughly the pore space that can be occupied by water: from the geometry of the specimen (0.07 m in diameter, 0.4 m in height), the porosity of about 0.39 and the initial water saturation of about 0.55 the remaining pore space that can be occupied by water is 270 cm^3 (in both tests).

For the thermal gradient test the 2D model including permeable isolation materials has been used. The calculated evolution of water intake in the thermal gradient test (2D model) is also clearly below the measured evolution of water intake, compare Figure 4-7. The calculated water intake is valid only for the bentonite material in the model and does not include the isolation materials.

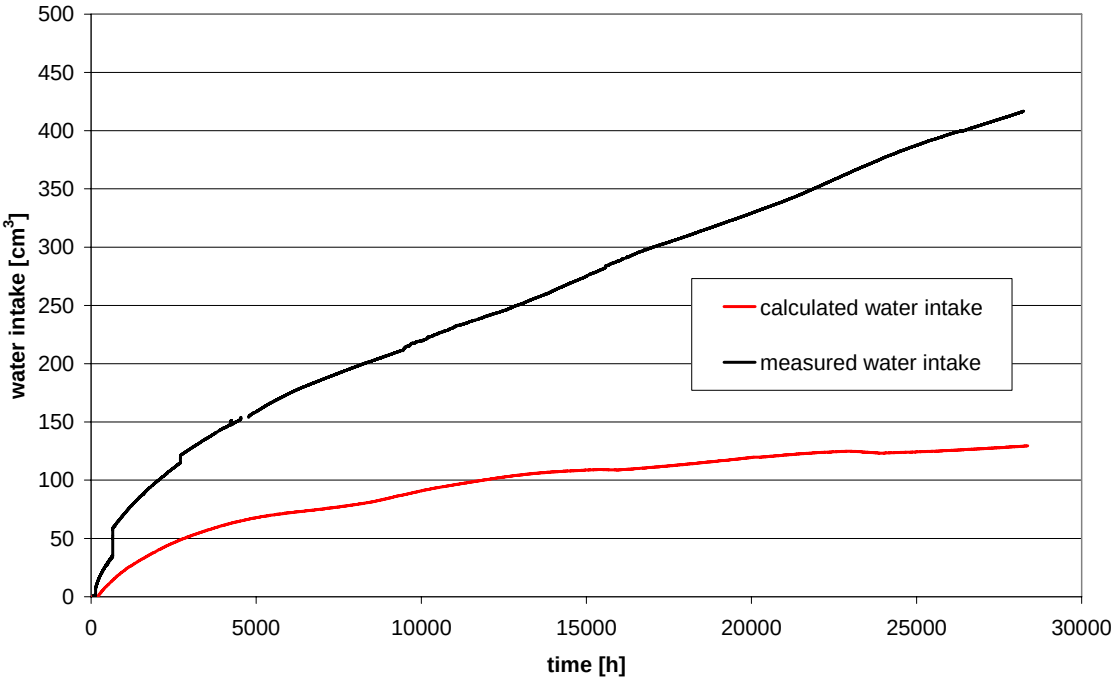

Figure 4-7. *Water intake evolution for the thermal gradient test.*

4.4 Discussion

The prediction of temperatures in the thermal gradient test cannot be modelled without taking into account the heat loss of the test equipment to the surrounding area. In the calculation reported here additional material groups and temperature boundary conditions have been used to model this heat loss and fit the measured with the calculated data.

For the prediction of relative humidity in the isothermal test a 1D two-phase-flow model has been used with a water pressure of 1.2 MPa at the upper end of the model and an air pressure of 0.1 MPa at the lower end as boundary condition. In the model for the thermal gradient test water can leave the specimen via the modelled isolation material. The tightness of the equipment is arguable, because the measured water intake is higher than theoretically possible (compare chapter 4.3.3) and it is not known where the point(s) of leakage are located (for imaginable possibilities compare Figure 4-1). Though the measured temperatures are matched well with the calculation (heat flow drives the vapour flow) the prediction of relative humidity and water intake is of limited significance due to the uncertainty of leakage.

5 Benchmark 1.1.3

As BM 1.1.3 for the project Task Force on Engineered Barrier Systems a laboratory experiment was chosen that was performed at the Technical University of Catalonia (UPC) in Spain with compacted FEBEX bentonite.

5.1 Experiment

Two cylindrical samples of compacted FEBEX bentonite were subjected for seven days to a prescribed heat flow of 2.17 W (for both specimens) from one end while the temperature was kept constant at 30 °C at the other end, see Figure 5-1. Temperatures were measured at various points along the axis of both specimens throughout the test. The two cylindrical specimens (0.038 m diameter, 0.076 m height) were placed vertically in the apparatus. The heater was located between the specimens. A latex membrane that allowed deformation and kept constant the overall water content and a layer (0.055 cm thickness) of heat insulating material surrounded the specimen. In order to ensure a good contact between the caps and the samples, a light stress (about 0.05 MPa) was applied on top of the test ensemble.

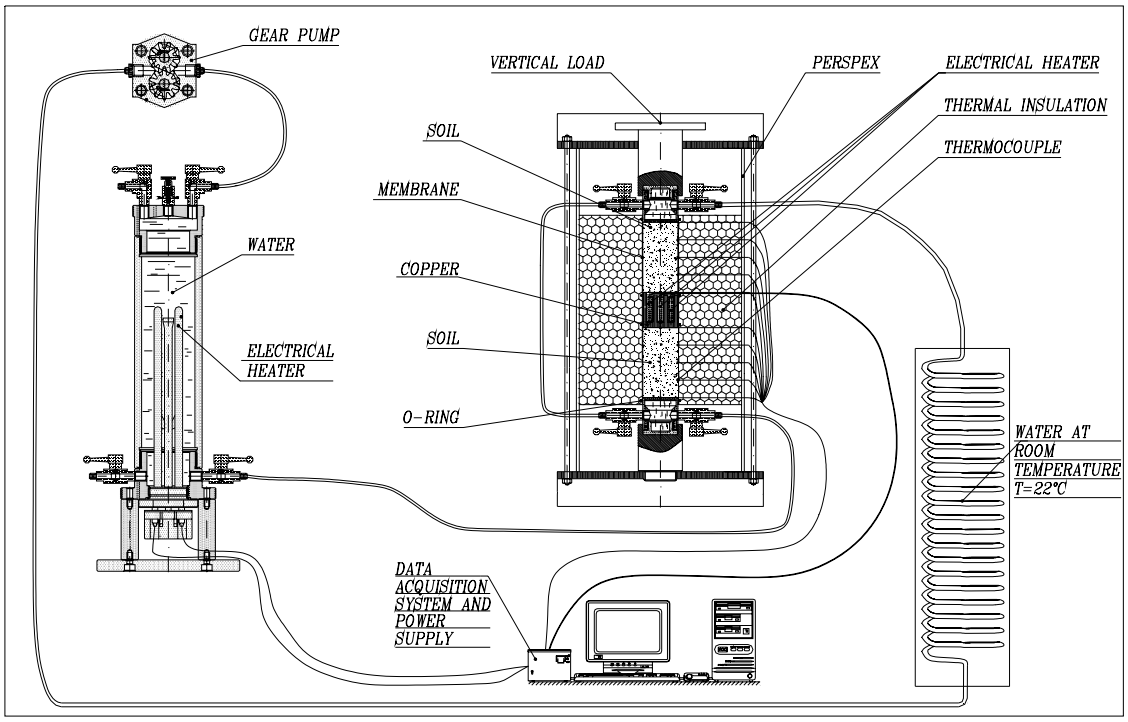

Figure 5-1. *Sketch of the experiment for BM 1.1.3 (UPC).*

After seven days the heater was switched off and the apparatus was dismantled. The diameter and water content at different points of the specimens were determined. The diameter of the specimen was measured at seven sections in each specimen with an accuracy of 0.01 mm. To obtain the distribution of the water content, each specimen was cut into six small cylinders, and the water content of each cylinder was determined.

The participants of BM 1.1.3 were asked to predict the evolution of measured values for temperature and the temperature distribution in the specimen for four points in time. Also the change of specimen diameter and the distribution of water content at the end of the test had to be predicted.

5.2 Model

For modelling the BM 1.1.3 one half of one of the two specimens was taken into account. The isolation material was included in the model. Axially symmetric elements have been implemented in GeoSys/RockFlow recently, but they were not used for modelling this benchmark because they are not sufficiently tested for non-isothermal unsaturated flow. The model was 2D (plain strain) as in the calculations for BM 1.1.1 and 1.1.2, see Figure 5-2.

A new feature of the code GeoSys/RockFlow allows an efficient calculation of coupled processes: the possibility to deactivate the calculation of processes in specified subdomains of the model. The complete set of THM-processes as documented in chapter 2 was calculated only in the subdomain that represents the bentonite specimen. In the subdomain for the isolation only heat conduction and deformation were calculated.

The initial temperature of the specimens was 22 °C. The specimens had a dry density of 1.63 g/cm3 and a water content of 15.33% (degree of saturation of 0.63).

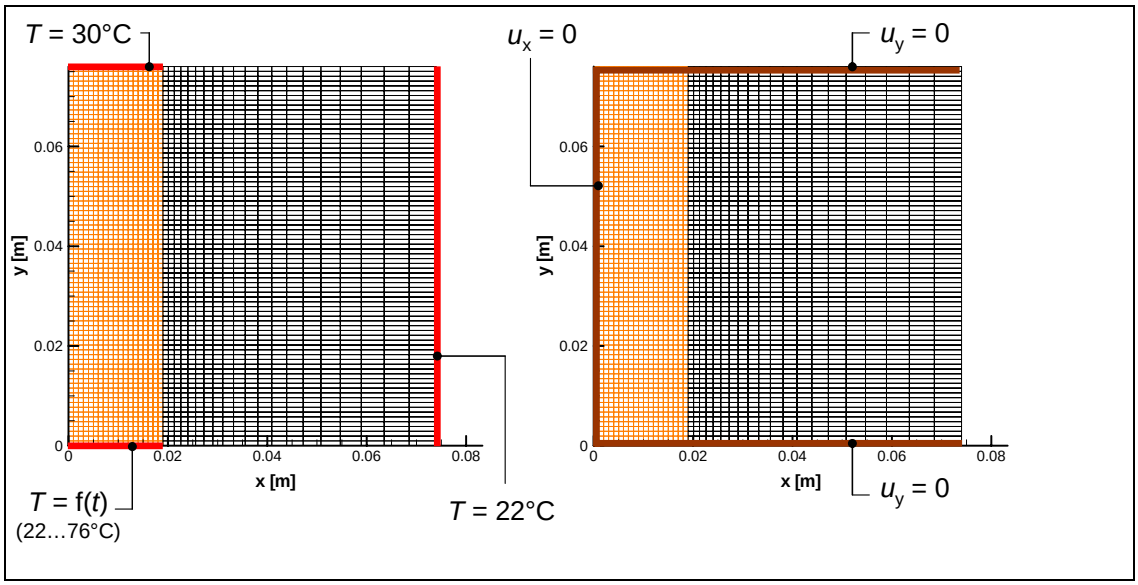

Figure 5-2. *Model for BM 1.1.3: boundary conditions for temperature and displacement.*

The parameter values for the FEBEX bentonite were taken as indicated in Table 5-1. The suction curve was chosen as in the calculations for BM 1.1.2 to fit the empirical relation of water content and suction in VILLAR et al. (2005), compare Figure 5-3.

The temperature change was the driving force for the redistribution of water content in the specimen and therefore also for the swelling process. In principle the use of a heat source is possible with GeoSys/RockFlow, but instead the measured temperatures at the heated end of the specimens were taken as boundary condition to simplify matters. As mentioned before the model was calculated in 2D and not axially symmetric, so the adjustment of heat loss via the isolation to the surrounding of the model would not have given results that are comparable to the experiment.

The same problem occurs for the (swelling) deformation of the specimen which was measured as a change of diameter. A 2D calculation results in a value for plain strain deformation.

A variation of parameter values was performed for permeability k and tortuosity τ. Tortuosity was reduced from the value of 1 (that had also been used for the thermal gradient test with FEBEX bentonite in BM 1.1.2) down to 0.8, 0.6, and 0.4. Afterwards additional calculations were performed with $\tau = 1$ for identical values of the ratio τ/k. For example, tortuosity value 0.8 divided by permeability value $3 \cdot 10^{-21}$ results in $2.67 \cdot 10^{20}$. That means, if tortuosity is 1 permeability value is $3.75 \cdot 10^{-21}$.

Table 5-1. Parameter values for FEBEX bentonite in BM 1.1.3.

parameter	**value**
permeability [m^2]	$3...7.5 \cdot 10^{-21}$
porosity [-]	0.39
tortuosity [-]	0.4...1.0
rel. permeability [-]	$k_{rel} = S_w^3$
heat conductivity [W/(m*K)]	0.95
heat capacity [J/(kg*K)]	426
Young's modulus [MPa]	31.7 MPa
Poisson's ratio [-]	0.3
thermal expansion coefficient [K^{-1}]	$1 \cdot 10^{-5}$
max. swelling pressure [MPa]	8.17

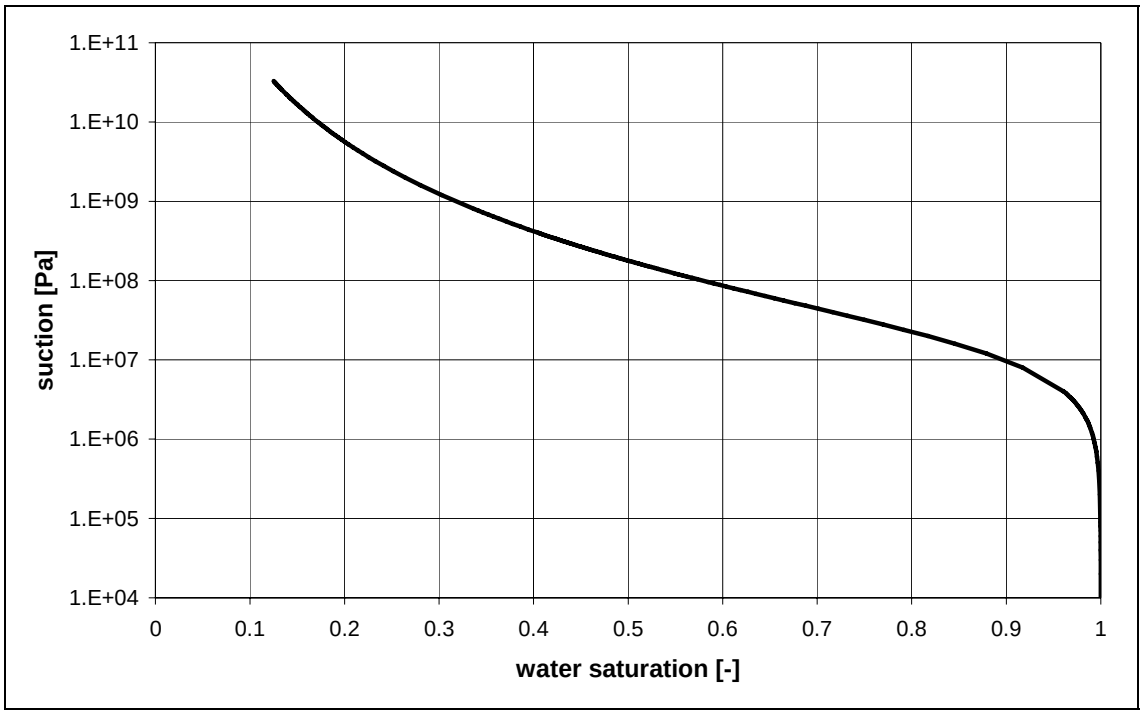

Figure 5-3. *Suction curve for BM 1.1.3.*

5.3 Results

Figure 5-4 shows the comparison of measured and calculated temperature evolutions (for $k = 3 \cdot 10^{-21}$ m^2 and $\tau = 1$). The calculated temperature evolution (red symbols) for all sensors agrees well with the measured evolution (congruent black symbols and lines). This result is not surprising as the system - both in the laboratory and in the model - was governed by the boundary conditions. The calculated temperatures are in principle influenced by the degree of water saturation. However, in the case of BM 1.1.3 the results from the other calculations hardly differ from the calculation with $k = 3 \cdot 10^{-21}$ m^2 and $\tau = 1$. The measured values at y = 0 mm (black line, heated end of the specimen) were used as boundary condition. The temperature at y = 76 mm (symbol: black diamond) was set to 30 °C which is close to the measured values.

Figure 5-5 shows the requested distribution plots for temperature.

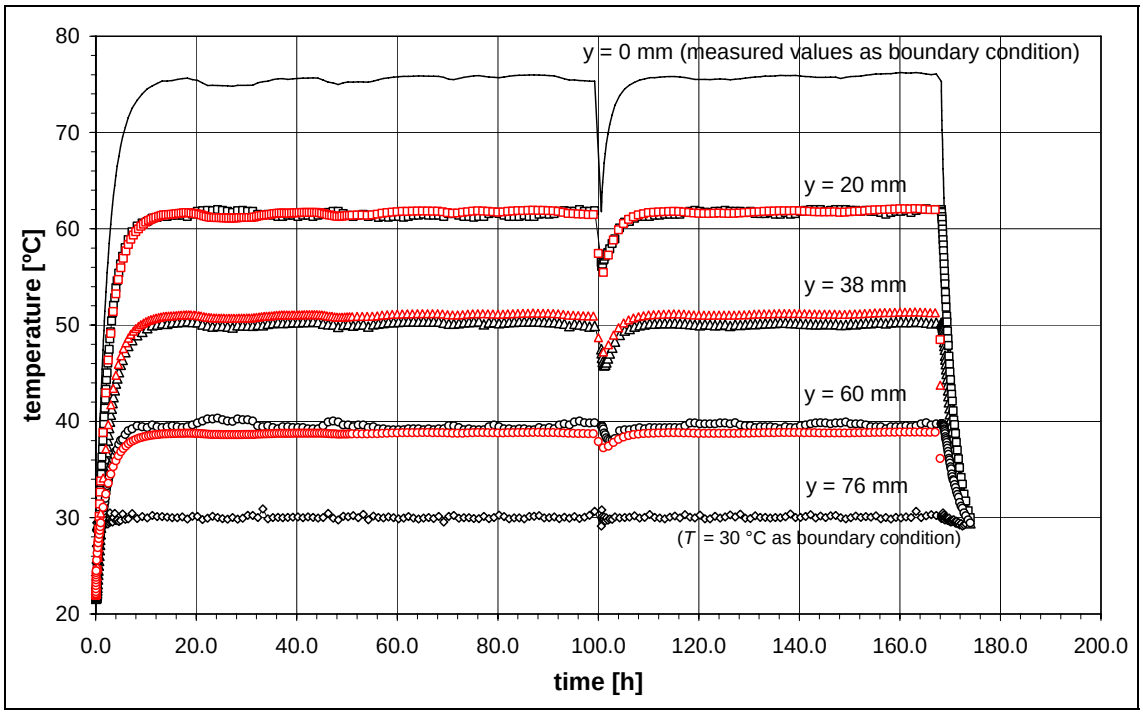

Figure 5-4. *Temperature evolution.*

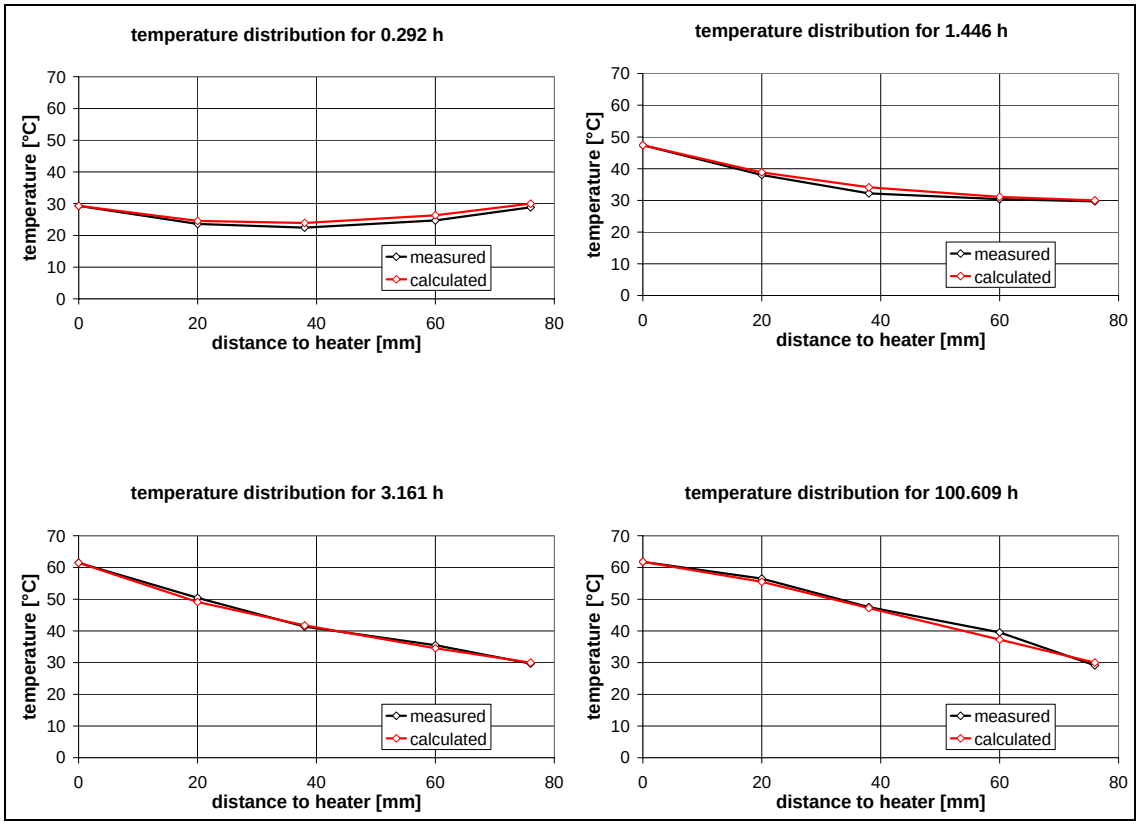

Figure 5-5. *Temperature distributions.*

Figure 5-6 shows the distribution of measured water content at the end of the test and the calculated water content after 168 h. The complete experiment included additional eight hours for cooling the specimen down to about 30 °C before water content was measured (compare Figure 5-4). The calculation results with identical τ/k-ratios are marked with equal symbols but different colours (red and blue).

The water content was the measured value of interest for BGR's modelling work, because the modelling of BM 1.1.3 in 2D instead of axially symmetric or 3D has no impact on the calculated water content (in contrast to the calculated deformations). The calculations were performed with varying values of permeability and tortuosity. The permeability value affects the movement of liquid water, the tortuosity value affects the movement of vapour, compare chapter 2.1.

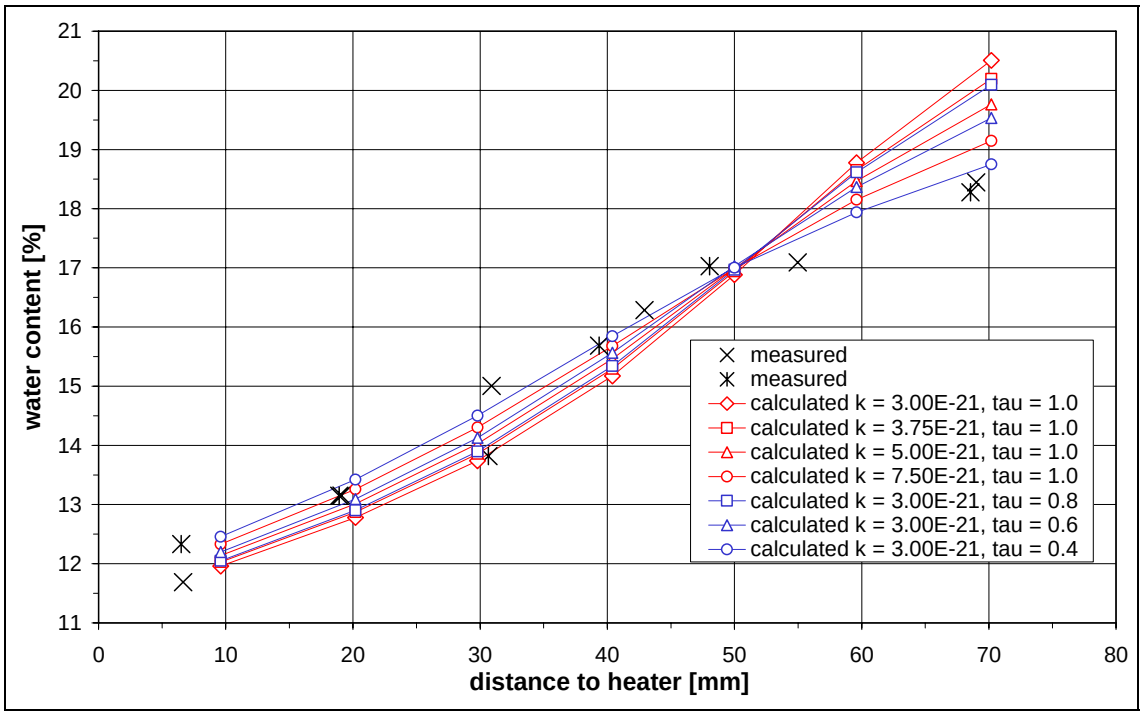

Figure 5-6. *Water content.*

Swelling deformation was calculated like in BM 1.1.1 (compare chapter 3) which was an example of confined swelling deformation. In case of free swelling this formulation has to be considered as an approximation: the parameter values that can be used to fit measured and calculated data are the swelling pressure and the elastic parameters Young's modulus and Poisson's ratio. Additional mismatch between experiment and model comes from the geometry of the model (2D instead of axially symmetric or 3D). For this reason the only effort to adjust the model to displacements of comparable magnitude was to set Young's modulus to a value of 31.7 MPa (that is one tenth of the value for BM 1.1.1). Figure 5-7 shows the measured diameter increment in comparison to the calculated x-displacement (plain strain model) of the contact specimen/isolation (calculation case: $k = 3 \cdot 10^{-21}$ m^2 and $\tau = 1$).

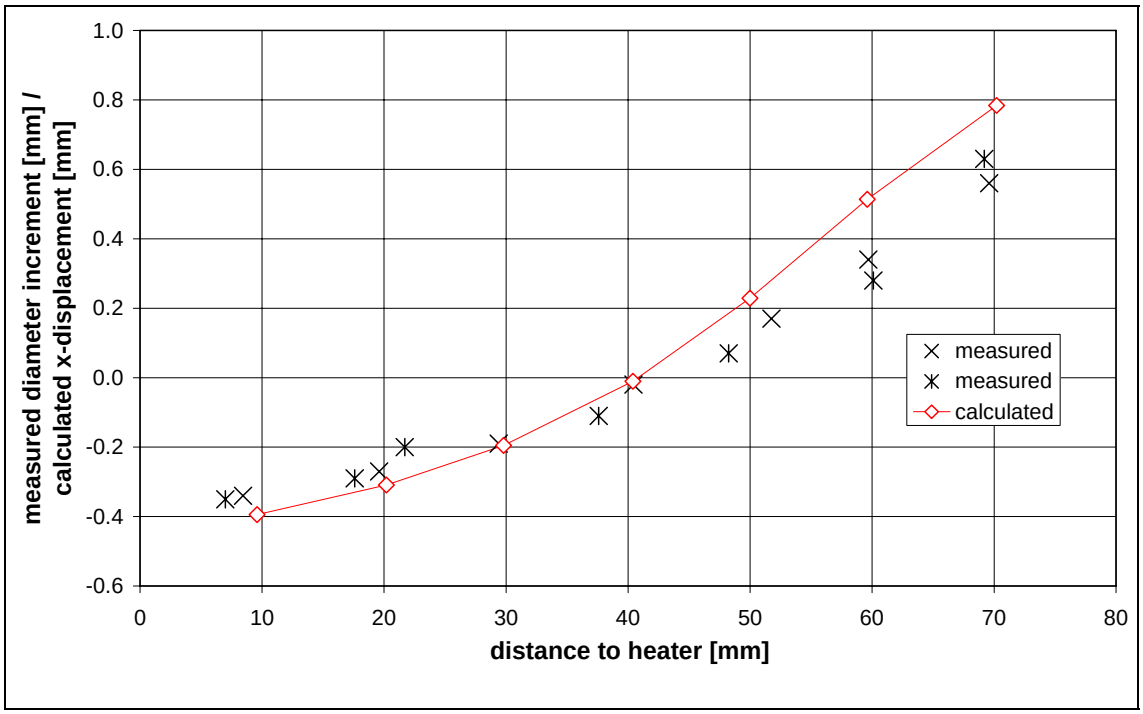

Figure 5-7. *Diameter increment / displacement.*

5.4 Mass conservation

In order to check the calculation results if mass conservation was (approximately) kept a special post-processing routine was implemented in the tool GINA4 from BGR. In case of BM 1.1.3 all boundaries of the model were closed and only a redistribution of the water in the model should occur. The initial amount of water in the model was taken as reference equal to 100%. Figure 5-8 shows the development of relative water mass in the model over the calculated time.

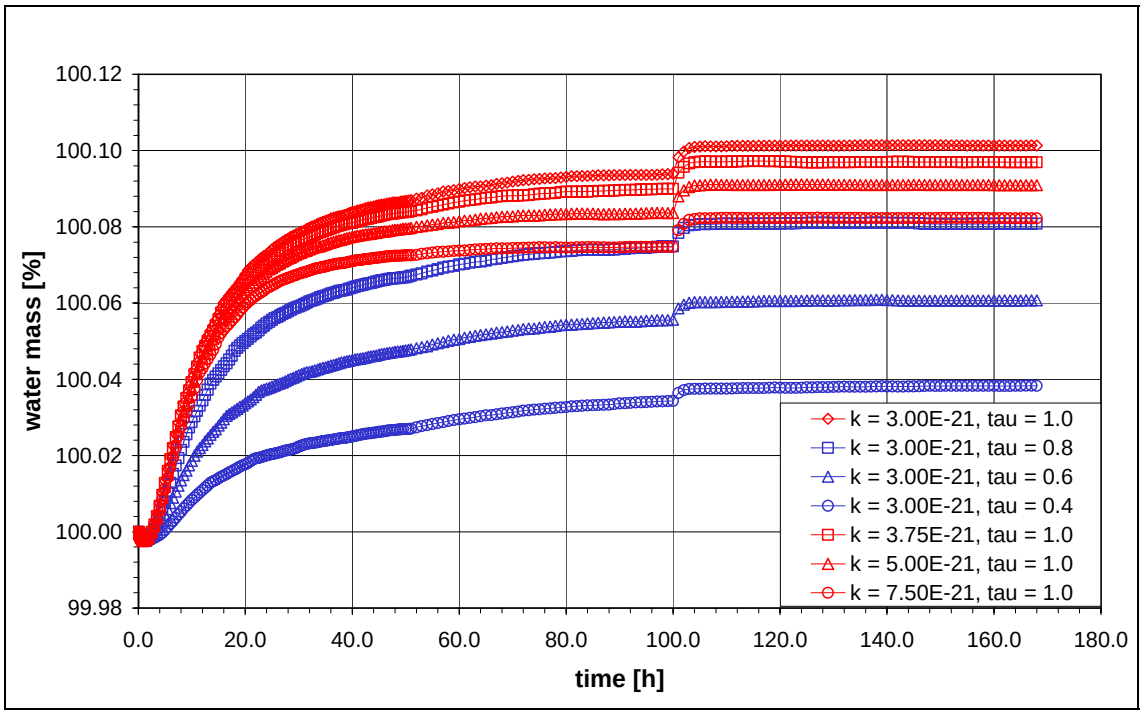

Figure 5-8. *Mass conservation.*

The sudden (but small) increase of water mass in the model after about 100 h coincides with a sudden decrease of temperature, compare Figure 5-4. At the end of the calculation there is a deviation of about 0.1 % at maximum compared to the initial water mass. For this reason the numerical approximation is considered to be acceptable. It is noticeable that the biggest (but still small) deviations occurs in the calculations where the flow of water vapour is more pronounced ($\tau = 1$).

5.5 Discussion

The calculated temperatures agree well with the measured data. The distribution plots for temperature - especially for early time data, compare Figure 5-5 - show that the assumed values for heat conductivity of the bentonite specimen and 0.039 W/(m*K) for the isolation material are reasonable. For the end of the test the agreement is due to the small size of the model and the choice of boundary conditions (steady state temperature field).

The calculated water content shows similar distributions for equal values of the ratio τ/k. Best agreement between measured and calculated data is for the ratio τ/k of $1.33 \cdot 10^{20}$ which corresponds to a permeability value of $7.5 \cdot 10^{-21}$ m^2 and $\tau = 1$, but also to a permeability value of $3 \cdot 10^{-21}$ m^2 and $\tau = 0.4$. From the measured data at the end of the test it is not possible to decide which values for k and τ are most suitable for the specimen. A fitting of k and τ would have been possible with a measured evolution of water content (or relative humidity from which water content can be derived) at different points in the specimen: Figure 5-9 shows the calculated evolution of water content at three points in the specimen for a permeability value of $7.5 \cdot 10^{-21}$ m^2 with $\tau = 1$ and for a permeability value of $3 \cdot 10^{-21}$ m^2 with $\tau = 0.4$.

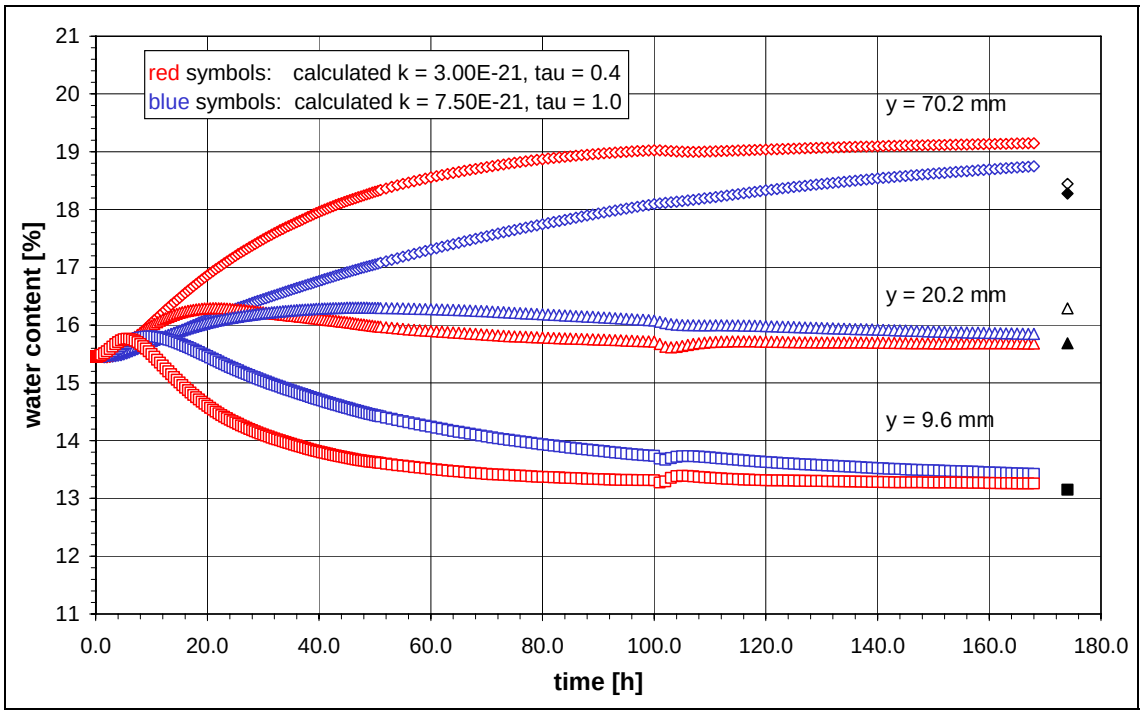

Figure 5-9. *Comparison of water content evolution for equal ratio τ/k.*

At the end of the test the calculated water contents at all three points in the specimen show only minor differences between the two calculations, but within the first three days of the calculated time the differences between the two assumptions for k and τ are clearly visible, especially for the point at y = 70.2 mm (near the cold end of the specimen).

A detailed interpretation of the calculated displacements in comparison to the measured diameter increments is not really worthwhile. First reason is that the 2D-geometry of the numerical model (plain strain) results in more pronounced displacements than in the experiment. The second weak point is the physical model: it accounts (only) for elastic material behaviour, and swelling pressure depending on water saturation is added. This means, that the calculated deformations only depend on the (constant) values for Young's modulus and Poisson's ratio. In the case of BM 1.1.1 – a confined bentonite specimen – this approach was sufficient to predict stresses caused by swelling. In the (special) case of free swelling as in BM 1.1.3 the adjustment of Young's modulus to fit the swelling deformations means that two different physical processes are merged into one (constant) parameter, so the calculation results basing on this approach have to be interpreted very carefully.

6 Summary

In 2004 the Swedish Nuclear Fuel and Waste Management Co. (SKB) initiated the project “Task Force on Engineered Barrier Systems”. This project has the objectives to verify the ability to model THM-coupled processes (Task 1) and gas migration processes (Task 2) in the clay-rich buffer materials. This report describes the modelling of the benchmarks concerning THM-coupled processes in geotechnical barriers (MX80 and FEBEX bentonite) with the code GeoSys/RockFlow at laboratory scale (benchmarks 1).

The experiments with MX80 (BM 1.1.1) require the treatment of vapour diffusion at temperatures of up to 150 °C. The measured data from BM 1.1.1 can be reproduced with the code, in most cases quantitatively, in few cases only qualitatively. Agreement between measured data and calculated data may be enhanced by adjusting parameter values.

The measured data from the experiments with FEBEX bentonite (BM 1.1.2) can be reproduced with the code, but uncertainties (leakages) in the experiment have been included in the corresponding models. For this reason the results from BM 1.1.2 are of limited significance.

The calculation of thermal and hydraulic processes succeeded very well for BM 1.1.3, whereas the results with respect to the mechanical processes are of limited significance. One reason is the model geometry. A 2D-model (plain strain) was applied to BM 1.1.3 which is in fact an axially symmetric problem. Axially symmetric elements have been implemented in GeoSys/RockFlow (after the modelling of BM 1.1.1 and 1.1.2 had been finished), and 3D elements are also available. These element types were tested successfully for several physical processes (for example single phase flow or mechanical deformation), but not for unsaturated flow which is a crucial process for the THM-benchmarks in this project; work on that topic is in progress.

The second reason for the limited significance of the mechanical results is the treatment of swelling in the code GeoSys/RockFlow. The development of the code is governed by the needs in the project DECOVALEX IV. The approach that was implemented in that framework was designed for the case of confined swelling and proofed to be appropriate in Task D of DECOVALEX IV (WANG et al. 2005) and also in the BM 1.1.1. For the case of free swelling calculation results basing on this approach have to be interpreted very carefully.

7 References

Gatabin, C. & Billaud, P. (2005): Bentonite THM Mock-up Experiments. Sensors Data Report. CEA, Technical Report **NT DPC/SCCME 05-300-A**: 47 p., 42 fig., 12 tab.; Gif sur Yvette (France).

Thorenz, C. (2000): Model Adaptive Simulation of Multiphase and Density Driven Flow in Fractured and Porous Media.University of Hanover, Institute for Fluid Mechanics ISEB; Hannover (Germany)

Villar, M. V., Martin, P. L. & Barcala, J. M. (2005): Infiltration Tests at Isothermal Conditions and under Thermal Gradient. Technical Report. Research Center for Energy, **CIEMAT/DMA/M2140/1/05**: 24 p., 15 fig., 8 tab.; Madrid (Spain).

Wang, W., Xie, M., Kolditz, O., Nowak, T., Kunz, H. & Shao, H. (2005): Progress on THM-analysis. 24 p., 29 fig., 2 tab. In: **Birkholzer, J., Rutqvist, J., Sonnenthal, E. & Barr, D. (2007)**: Task D, Long-Term Permeability/Porosity Changes in the EDZ and Near Field due to THM and THC Processes in Volcanic and Crystalline-Bentonite Systems, Appendix E. Swedish Nuclear Power Inspectorate, SKI-Report 2007:10; Stockholm (Sweden)